Computational Chemistry Applied in the Analyses of

Chitosan/ Polyvinylpyrrolidone/ *Mimosa Tenuiflora*

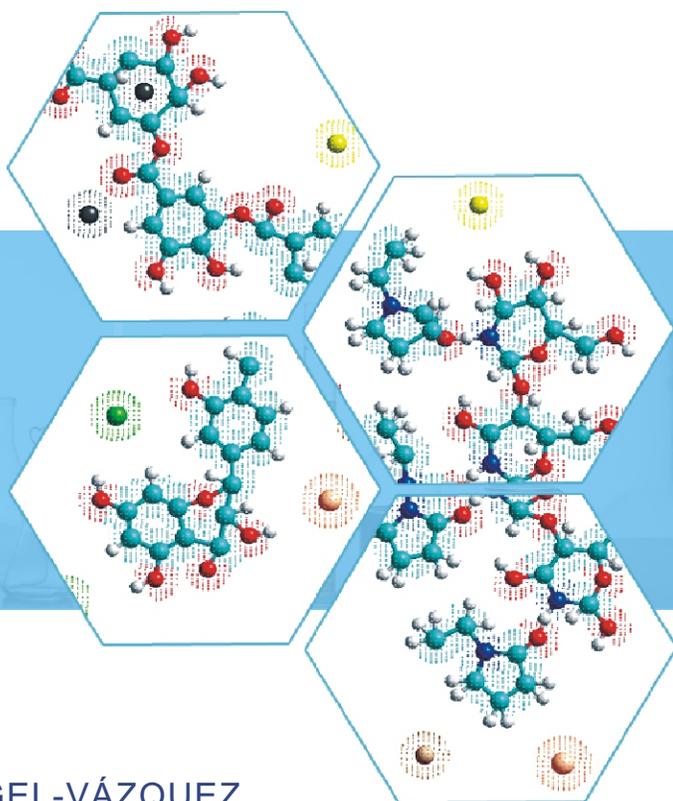NORMA AUREA RANGEL-VÁZQUEZ
FRANCISCO RODRÍGUEZ FÉLIX

Computational Chemistry Applied in the Analyses of Chitosan/ Polyvinylpyrrolidone/ *Mimosa Tenuiflora*
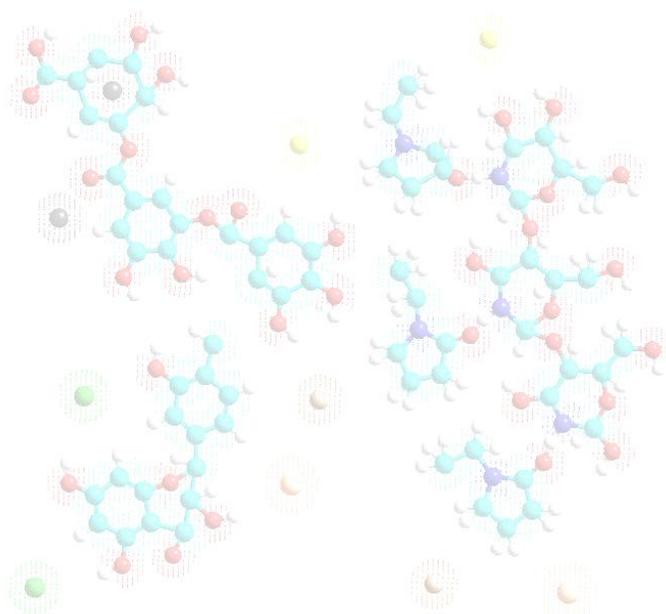
NORMA AUREA RANGEL-VÁZQUEZ

FRANCISCO RODRÍGUEZ FÉLIX

Science Publishing Group

548 Fashion Avenue
New York, NY 10018

http://www.sciencepublishinggroup.com

Published by Science Publishing Group 2014

First Edition

To order additional copies of this book, please contact:
Science Publishing Group
service@sciencepublishinggroup.com
http://www.sciencepublishinggroup.com

Printed and bound in India

Preface

Computational chemistry allows using various models analyze and predict the behavior of single and composite materials to determine the composition of new materials.

It should be noted that a model is a representation of the construction and working of some system of interest. A model is similar to but simpler than the system it represents. One purpose of a model is to enable the analyst to predict the effect of changes to the system. On the one hand, a model should be a close approximation to the real system and incorporate most of its salient features. On the other hand, it should not be so complex that it is impossible to understand and experiment with it. A good model is a judicious tradeoff between realism and simplicity.

This book is aimed at researchers and students with basic knowledge of computational chemistry, interested in analyzing and discussing the structural properties of different polymers. It should be noted that this book is carried out an analysis of polymers such as Chitosan, PVP and MT as well as the structure of the model from the mixture of these polymers using a computational analysis using a comparison between PM3 and AM1 semi-empirical methods, respectively.

In this case, Chitosan is a linear polysaccharide composed of randomly distributed β-(1-4)-linked D-glucosamine (deacetylated unit) and N-acetyl-D-glucosamine (acetylated unit). It is made by treating shrimp and other crustacean shells with the alkali sodium hydroxide. Chitosan has a number of commercial and possible biomedical uses. It can be used in agriculture as a seed treatment and biopesticide, helping plants to fight off fungal infections. In winemaking it can be used as a fining agent, also helping to prevent spoilage. In industry, it can be used in a self-healing polyurethane paint coating. In medicine, it may be useful in bandages to reduce bleeding and as an antibacterial agent; it can also be used to help deliver drugs through the skin.

PVP was first synthesized by Walter Reppe and a patent was filed in 1939 for one of the most interesting derivatives of acetylene chemistry. PVP was initially used as a blood plasma substitute and later in a wide variety of applications in medicine, pharmacy, cosmetics and industrial production. It is used as a binder in many pharmaceutical tablets; it simply passes through the body when taken

orally. However, autopsies have found that crospovidone does contribute to pulmonary vascular injury in substance abusers who have injected pharmaceutical tablets intended for oral consumption. The long-term effects of crospovidone within the lung are unknown. PVP added to iodine forms a complex called povidone-iodine that possesses disinfectant properties. This complex is used in various products like solutions, ointment, pessaries, liquid soaps and surgical scrubs. It is known under the trade name Betadine and Pyodine. It is used in pleurodesis (fusion of the pleura because of incessant pleural effusions). For this purpose, povidone iodine is equally effective and safe as talc, and may be preferred because of easy availability and low cost.

Finally, *Mimosa tenuiflora*, syn. *Mimosa hostilis* (Jurema, Tepezcohuite) is a perennial tree or shrub native to the northeastern region of Brazil (Para ba, Rio Grande do Norte, Cear á Pernambuco, Bahia) and found as far north as southern Mexico (Oaxaca and coast of Chiapas). It is most often found in lower altitudes, but it can be found as high as 1000 m. *Mimosa tenuiflora* is a very good source of fuel wood and works very well for making posts, most likely because of its high tannin content (16%), which protects it from rot.

Due to its high tannin content, the bark of the tree is widely used as a natural dye and in leather production. It is used to make bridges, buildings, fences, furniture and wheels. It is an excellent source of charcoal and at least one study has been done to see why this is the case.

Finally, an important difference that has this book is, the analysis and determination of properties such as FTIR, electrostatic potentials and structural parameters of polymers in an individual way and in union, to propose a structure for a new material that has great features to be applied in the medical field and thus contribute to a need in society in general.

Acknowledgements

God, for giving me the opportunity to live each day despite the adversities that are taken on the road.

At RRA (+) I don't have words to thank you despite your early absence always give me strength and energy to move forward.

At my future BB and my family, love will always are the most important in my life, the greatest gift that God gave me.

At M.E. Dora Luz Arriaga Soto (Director of ITA) and M. A. Isabel Álvarez Hernández (ITA) for your invaluable friendship.

At my friends, Ph D. Adrian Bonilla, Ph D. Viky, Ph D Ana María Mendoza, Ph D. Carlos Sánchez, and M. Sc. Alejandra Ibeth. Thanks you for your invaluable friendship.

At Mani Soma (WSU): you are a great person, thank you for your comments and specially for your invaluable friendship.

Contents

Chapter 1

Molecular Modelation

Chapter 1

Molecular Modelation

NORMA AUREA RANGEL-VÁZQUEZ

División de Estudios de Posgrado e Investigación del Instituto Tecnológico de Aguascalientes, Ave. López Mateos # 1801 Ote. Fracc. Bona Gens CP. 20256 Aguascalientes, Aguascalientes, México

Abstract

Model is the process of producing a model; a model is a representation of the construction and working of some system of interest. A model is similar to but simpler than the system it represents. One purpose of a model is to enable the analyst to predict the effect of changes to the system. On the one hand, a model should be a close approximation to the real system and incorporate most of its salient features. On the other hand, it should not be so complex that it is impossible to understand and experiment with it. A good model is a judicious tradeoff between realism and simplicity.

Simulation practitioners recommend increasing the complexity of a model iteratively. An important issue in modeling is model validity. Model validation techniques include simulating the model under known input conditions and comparing model output with system output. Generally, a model intended for a simulation study is a mathematical model developed with the help of simulation software. Mathematical model classifications include deterministic (input and output variables are fixed values) or stochastic (at least one of the input or output variables is probabilistic); static (time is not taken into account) or dynamic (time-varying interactions among variables are taken into account). Typically, simulation models are stochastic and dynamic.

Keywords: Modelling, PM3, AM1, Simulation

1.1 Introduction

Attractive interactions between π systems are one of the principal noncovalent forces governing molecular recognition and play important roles in many chemical and biological systems. Attractive interaction between π systems is the interaction between two molecules leading to self-organization by formation of a complex structure which has lower conformation equilibrium than of the separate components and shows different geometrical arrangement with high percentage of yield. It is known that many aromatic compounds form infinite stacks with parallel molecular planes when crystallized.

Hydrogen bonding, electrostatic interactions, van der Waals interactions (van der Waals bonds are mainly constructed with a balance of the exchange repulsion and dispersion attractive interactions), donor–acceptor interactions, hydrophilic–hydrophobic interactions, and π−π interactions are the main types of non-covalent interactions that are responsible for self-organization in biological systems. A lot of experimental evidence of charge transfer (CT) complexes had been reported in solid or in solution in a different field of chemistry. According to Mulliken's theory, formation of the (CT) complex involves transition of an electron from HOMO of donor to LUMO of acceptor.

Opposing π systems typically adopt a parallelplaner (stacked or offset-stacked) geometry. The interaction between the donor and acceptor is characteristic of an electronic absorption band with low energy. One of these molecular complexes is π, π-complex between neutral molecules.

Quantum chemical calculations are applied to study the (CT) complexes in order to obtain information on structures and other molecular properties like specific interaction of donor and acceptor. The interaction energy contribution comes from the effects of donor–acceptor interactions and π−π interactions. The self-assembly of these molecular systems was studied using quantum mechanical semi-empirical methods in gas phase. The minimum energy configuration of the stacked molecular systems were investigated by geometry optimizations and then the other properties, such as stacking distances, heat of formation, dipole moment, and polarizability were also calculated [1].

1.2 Molecular Mechanics

The mechanical molecular model considers atoms as spheres and bonds as springs. The mathematics of spring deformation can be used to describe the

ability of bonds to stretch, bend, and twist (Figure 1.1).
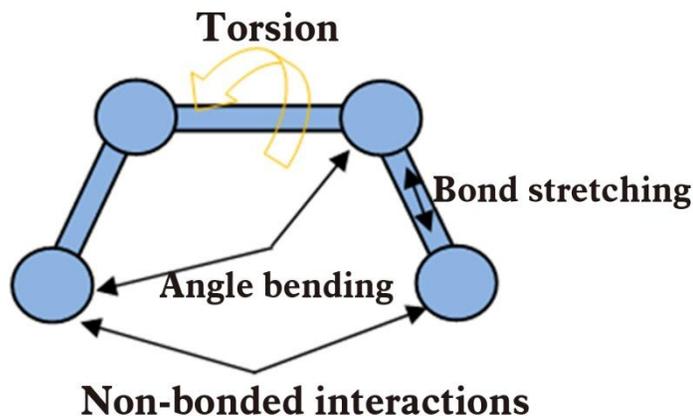
Figure 1.1 *The mechanical molecular model.*

Non-bonded atoms (greater than two bonds apart) interact through van der Waals attraction, steric repulsion, and electrostatic attraction/repulsion. These properties are easiest to describe mathematically when atoms are considered as spheres of characteristic radii. The object of molecular mechanics is to predict the energy associated with a given conformation of a molecule. However, molecular mechanics energies have no meaning as absolute quantities. Only differences in energy between two or more conformations have meaning. A simple molecular mechanics energy equation (1) is given by:

$$\text{Energy} = \text{Stretching Energy} + \text{Bending Energy} + \text{Torsion Energy} + \text{Non} - \text{Bonded Interaction Energy} \tag{1}$$

These equations (1) together with the data (parameters) required to describe the behavior of different kinds of atoms and bonds, is called a force-field. Many different kinds of force-fields have been developed over the years. Some include additional energy terms that describe other kinds of deformations. Some force-fields account for coupling between bending and stretching in adjacent bonds in order to improve the accuracy of the mechanical model. The mathematical form of the energy terms varies from force-field to force-field. The more common forms will be described [2].

- Stretching Energy

The stretching energy equation is based on Hooke's law. The "kb" parameter controls the stiffness of the bond spring, while "ro" defines its equilibrium

length. Unique "kb" and "ro" parameters are assigned to each pair of bonded atoms based on their types (e.g. C-C, C-H, O-C, etc.). Where "r" is the distance between two atoms, this equation (2) estimates the energy associated with vibration about the equilibrium bond length. This is the equation of a parabola (Figure 1.2), as can be seen in the following plot.

$$E = \sum_{bonds} k_b (r - r_o)^2 \qquad (2)$$
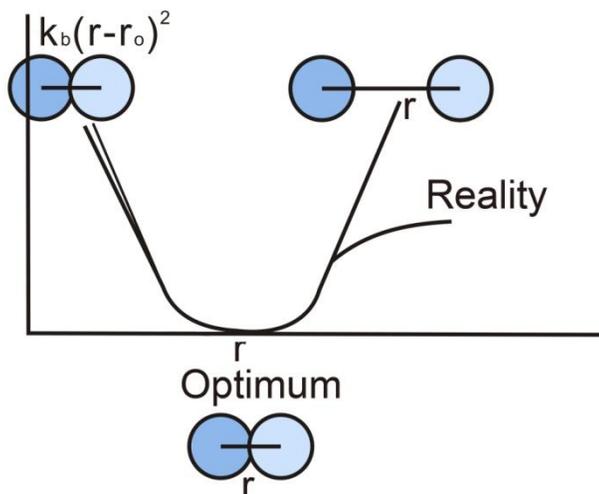
Figure 1.2 *Equation of parabola.*

Notice that the model tends to break down as a bond is stretched toward the point of dissociation [2].

- Bending Energy

The bending energy equation is also based on Hooke's law. The "k*theta*" parameter controls the stiffness of the angle spring, while "theta*o*" defines its equilibrium angle (Figure 1.3). This equation (3) estimates the energy associated with vibration about the equilibrium bond angle.

$$E = \sum_{angles} k_\theta (\theta - \theta_o)^2 \qquad (3)$$
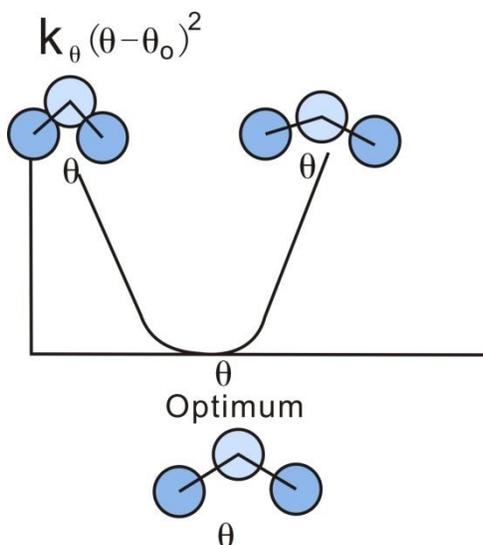
Figure 1.3 Parabola graphic.

Unique parameters for angle bending are assigned to each bonded triplet of atoms based on their types (e.g. C-C-C, C-O-C, C-C-H, etc.). The effect of the "k*b*" and "k*theta*" parameters is to broaden or steepen the slope of the parabola. The larger the value of "k", the more energy is required to deform an angle (or bond) from its equilibrium value. Shallow potentials are achieved for "k" values between 0.0 and 1.0 [2]. The Hookeian potential is shown in the following plot for three values of "k" (Figure 1.4).
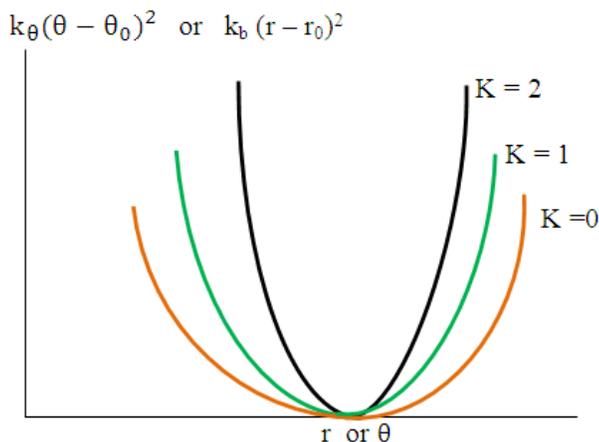
Figure 1.4 Hookein potential.

- Torsion Energy

Intramolecular rotations (rotations about torsion or dihedral angles) require energy (equation 4 and Figure 1.5). Torsional energies are usually important only for single bonds because double and triple bonds are too rigid to permit rotation.

$$E = \sum_{torsions} A\left[1 + \cos(n\tau - \phi)\right] \tag{4}$$
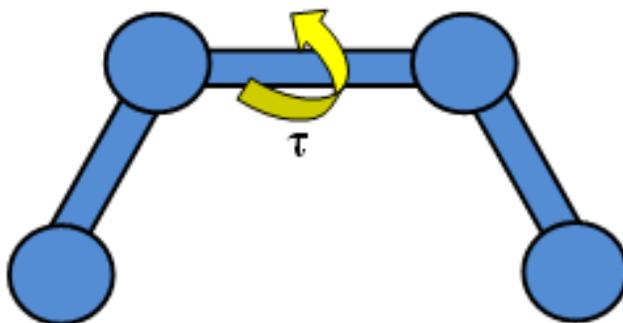
Figure 1.5 Torsion bond.

The torsion energy in molecular mechanics is primarily used to correct the remaining energy terms rather than to represent a physical process. The torsional energy represents the amount of energy that must be added to or subtracted from the Stretching Energy + Bending Energy + Non-Bonded Interaction Energy terms to make the total energy agree with experiment or rigorous quantum mechanical calculation for a model dihedral angle (ethane, for example might be used a model for any H-C-C-H bond). The "A" parameter controls the amplitude of the curve, the n parameter controls its periodicity, and "phi" shifts the entire curve along the rotation angle axis (tau). The parameters are determined from curve fitting. Unique parameters for torsional rotation are assigned to each bonded quartet of atoms based on their types (e.g. C-C-C-C, C-O-C-N, H-C-C-H, etc.) (Equation 4). Torsion potentials with three combinations of "A", "n", and "phi" are shown in the following Figure 1.6.

$A[1 + \cos\ (n\tau\ -\ \Phi)$

1) $A=2$, $\quad n=2$, $\quad \Phi=0^0$
2) $A=1$, $\quad n=2$, $\quad \Phi=0^0$
3) $A=1$, $\quad n=1$, $\quad \Phi=90^0$

1)

2)

3)
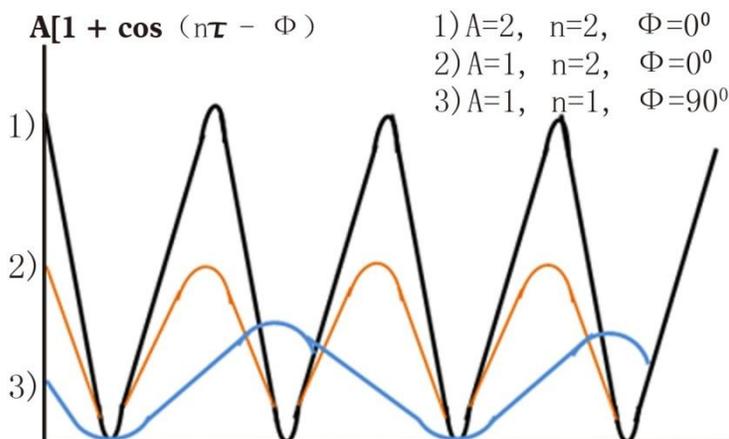
Figure 1.6 Torsion potentials with three combinations.

Notice that "n" reflects the type symmetry in the dihedral angle. A CH_3-CH_3 bond, for example, ought to repeat its energy every 120 degrees. The *cis* conformation of a dihedral angle is assumed to be the zero torsional angles by convention. The parameter phi can be used to synchronize the torsional potential to the initial rotameric state of the molecule whose energy is being computed [2].

- Non-Bonded Energy

The non-bonded energy represents (equation 5) the pair-wise sum of the energies of all possible interacting non-bonded atoms i and j (Figure 1.7).

$$E = \Sigma_i \Sigma_j - \frac{A_{ij}}{r_{ij}^6} + \frac{B_{ij}}{r_{ij}^{12}} + \Sigma_i \Sigma_j \frac{q_i q_j}{r_{ij}} \tag{5}$$

van der Waals term   Electrostatic term
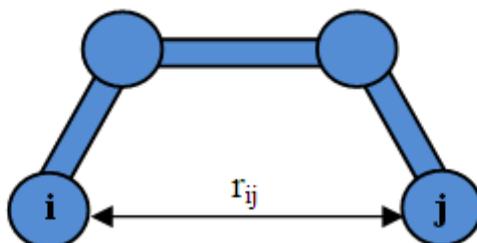
Figure 1.7 Non-bonded atoms i and j.

The non-bonded energy accounts for repulsion, van der Waals attraction, and electrostatic interactions (Figure 1.8). Van der Waals attraction occurs at short range, and rapidly dies off as the interacting atoms move apart by a few Angstroms. Repulsion occurs when the distance between interacting atoms becomes even slightly less than the sum of their contact radii. Repulsion is modeled by an equation that is designed to rapidly blow up at close distances (1/r^12 dependency). The energy term that describes attraction/repulsion provides for a smooth transition between these two regimes.
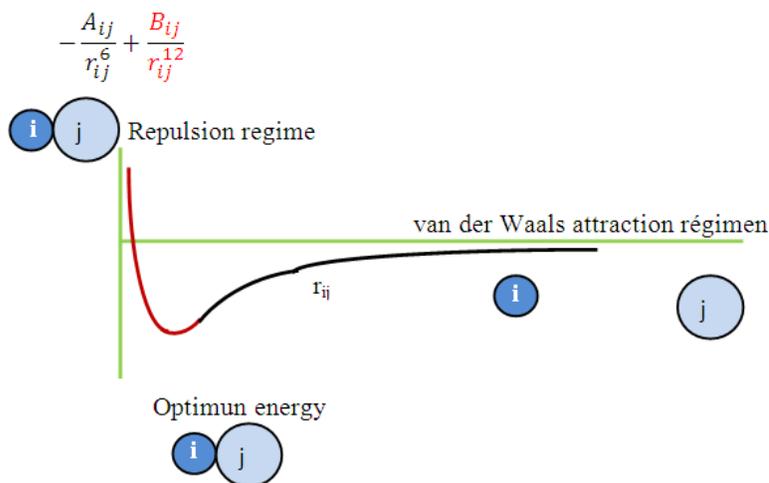
Figure 1.8 *Van der Waals and electrostatic attractions.*

The "A" and "B" parameters control the depth and position (interatomic distance) of the potential energy (Figure 1.9) well for a given pair of non-bonded interacting atoms (e.g. C:C, O:C, O:H, etc.). In effect, "A" determines the degree of "stickiness" of the van der Waals attraction and "B" determines the degree of "hardness" of the atoms (e.g marshmallow-like, billiard ball-like, etc.).

$$-\frac{A_{ij}}{r_{ij}^{6}} + \frac{B_{ij}}{r_{ij}^{12}}$$

A = 0.5   B = 1

A = 1   B = 0.5

r_{ij}
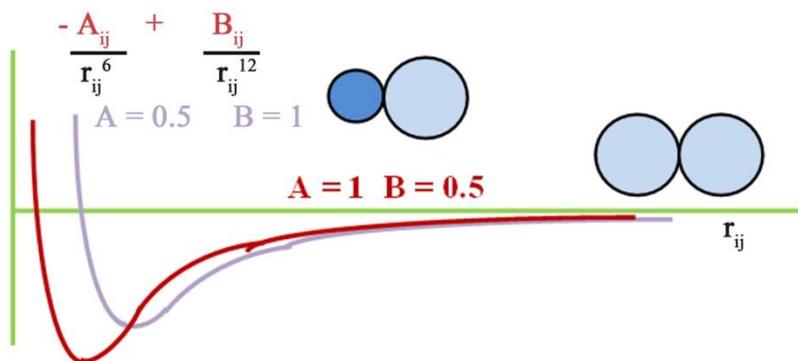
Figure 1.9 *A and B parameters control of the potential energy.*

The "A" parameter can be obtained from atomic polarizability measurements, or it can be calculated quantum mechanically. The "B" parameter is typically derived from crystallographic data so as to reproduce observed average contact distances between different kinds of atoms in crystals of various molecules. The electrostatic contribution is modeled using a Coulombic potential. The electrostatic energy is a function of the charge on the non-bonded atoms, their interatomic distance, and a molecular dielectric expression that accounts for the attenuation of electrostatic interaction by the environment (e.g. solvent or the molecule itself). Often, the molecular dielectric is set to a constant value between 1.0 and 5.0. A linearly varying distance-dependent dielectric (i.e. 1/r) is sometimes used to account for the increase in environmental bulk as the separation distance between interacting atoms increases. Partial atomic charges can be calculated for small molecules using an *ab initio* or semiempirical quantum technique (usually MOPAC or AMPAC). Some programs assign charges using rules or templates, especially for macromolecules. In some force-fields, the torsional potential is calibrated to a particular charge calculation method (rarely made known to the user). Use of a different method can invalidate the force-field consistency [2].

AMBER Method

The term "AMBER force field" generally refers to the functional form used by the family of AMBER force fields. This form includes a number of parameters; each member of the family of AMBER force fields provides values for these parameters and has its own name. The functional form of the AMBER force field is (equation 6).

$$
\begin{aligned}
V(\tau^N) = &\sum_{bonds} k_b (1 - 1_0)^2 + \sum_{angles} k_a (\theta - \theta_0)^2 \\
&+ \sum_{angles} 0.5\, V_N \left[1 + \cos(nw - \gamma) \right] \\
&+ \sum_{j=1}^{N-1} \sum_{i=j+1}^{N} \left\{ o_{ij} \left(\frac{ro_{ij}}{r_{ij}} \right)^{12} - 2 \left(\frac{ro_{ij}}{r_{ij}} \right)^6 + \frac{q_i q_j}{4 \Pi \varepsilon_0 ro_{ij}} \right\}
\end{aligned}
\tag{6}
$$

The meanings of right hand side terms are:

1) First term (summing over bonds): represents the energy between covalently bonded atoms. This harmonic (ideal spring) force is a good approximation near the equilibrium bond length, but becomes increasingly poor as atoms separate.

2) Second term (summing over angles): represents the energy due to the geometry of electron orbitals involved in covalent bonding.

3) Third term (summing over torsions): represents the energy for twisting a bond due to bond order (e.g. double bonds) and neighboring bonds or lone pairs of electrons. Note that a single bond may have more than one of these terms, such that the total torsional energy is expressed as a Fourier series.

4) Fourth term (double summation over i and j): represents the non-bonded energy between all atom pairs, which can be decomposed into van der Waals (first term of summation) and electrostatic (second term of summation) energies.

The form of the van der Waals energy is calculated using the equilibrium distance (ro_{ij}) and well depth (ε). The factor of 2 ensures that the equilibrium distance is ro_{ij}. The energy is sometimes reformulated in terms of o, where $ro_{ij} = 2^{1/6}$ (o), as used e.g. in the implementation of the soft core potentials. The form of the electrostatic energy used here assumes that the charges due to the protons and electrons in an atom can be represented by a single point charge (or in the case of parameter sets that employ lone pairs, a small number of point charges) [3].

1.3 Semi-Empirical Methods

Semi-empirical quantum chemistry methods are based on the Hartree–Fock formalism, but make many approximations and obtain some parameters from empirical data. They are very important in computational chemistry for treating

large molecules where the full Hartree–Fock method without the approxima-
tions is too expensive. The use of empirical parameters appears to allow some
inclusion of electron correlation effects into the methods. Within the framework
of Hartree–Fock calculations, some pieces of information (such as two-electron
integrals) are sometimes approximated or completely omitted. In order to
correct for this loss, semi-empirical methods are parametrized, that is their
results are fitted by a set of parameters, normally in such a way as to produce
results that best agree with experimental data, but sometimes to agree with *ab
initio* results. Semi-empirical methods follow what are often called empirical
methods where the two-electron part of the Hamiltonian is not explicitly
included.

For π-electron systems, this was the Hückel method proposed by Erich
Hückel [4-6]. For all valence electron systems, the extended Hückel method
was proposed by Roald Hoffmann [7]. Semi-empirical calculations are much
faster than their *ab initio* counterparts. Their results, however, can be very
wrong if the molecule being computed is not similar enough to the molecules in
the database used to parametrize the method. Semi-empirical calculations have
been most successful in the description of organic chemistry, where only a few
elements are used extensively and molecules are of moderate size. However,
semi-empirical methods were also applied to solids [8] and nanostructures [9]
but with different parameterization. As with empirical methods, we can
distinguish methods that are: Restricted to π-electrons. These methods exist for
the calculation of electronically excited states of polyenes, both cyclic and
linear. These methods, such as the Pariser–Parr–Pople method (PPP), can
provide good estimates of the π-electronic excited states, when parameterized
well. Indeed, for many years, the PPP method outperformed ab initio excited
state calculations [10-11].

1.3.1 AM1 Method

AM1 is basically a modification to and a reparameterization of the general
theoretical model found in MNDO. Its major difference is the addition of
Gaussian functions to the description of core repulsion function to overcome
MNDO's hydrogen bond problem. Additionally, since the computer resources
were limited in 1970s, in MNDO parameterization methodology, the overlap
terms, βs and βp, and Slater orbital exponent's ζs and ζp for *s-* and *p-* atomic
orbitals were fixed. That means they are not parameterized separately just
considered as $\beta s = \beta p$, and $\zeta s = \zeta p$ in MNDO. Due to the greatly increasing
computer resources in 1985 comparing to 1970s, these inflexible conditions
were relaxed in AM1 and then likely better parameters were obtained.

The addition of Gaussian functions significantly increased the numbers of parameters to be parameterized from 7 (in MNDO) to 13-19, but AM1 represents a very real improvement over MNDO, with no increase in the computing time needed. Dewar also concluded that the main gains of AM1 were its ability to reproduce hydrogen bonds and the promise of better estimation of activation energies for reactions. However, AM1 has some limitations. Although hypervalent molecules are improved over MNDO, they still give larger errors than the other compounds, alkyl groups are too stable, nitro compounds are too unstable, peroxide bond are too short. AM1 has been used very widely because of its performance and robustness compared to previous methods. This method has retained its popularity for modeling organic compounds and results from AM1 calculations continue to be reported in the chemical literature for many different applications [12].

Theory

AM1 is currently one of the most commonly used of the Dewar-type methods. It was the next semiempirical method introduced by Dewar and coworkers in 1985 following MNDO. It is simply an extension, a modification to and also a reparameterization of the MNDO method. AM1 differs from MNDO by mainly two ways. The first difference is the modification of the core repulsion function. The second one is the parameterization of the overlap terms βs and βp, and Slater-type orbital exponents ζs and ζp on the same atom independently, instead of setting them equal as in MNDO. MNDO had a very strong tendency to overestimate repulsions between atoms when they are at approximately their van der Waals distance apart. To overcome this hydrogen bond problem, the net electrostatic repulsion term of MNDO, $f (R_{AH})$ given by equation (7), was modified in MNDO/H to be

$$f(R_{AH}) = Z_A Z_B (S_A S_A | S_H S_H) \left[e^{-\alpha R_{AH}^2} \right] \tag{7}$$

Where α was proposed to be equal to 2.0 Å^{-2} for all A-H pairs. On the other hand, the original core repulsion function of MNDO was modified in AM1 by adding Gaussian functions to provide a weak attractive force. The core-core repulsion energy term in AM1 is given by equation 8.

$$E_{AB}^{AM1} = Z_A Z_B (S_A S_A | S_H S_H) \left[1 + e^{-\alpha A R_{AB}} + e^{-\alpha B R_{AB}} \right]$$
$$+ \frac{Z_A Z_B}{R_{AB}} \left[F(A) + F(B) \right] \tag{8}$$

The Gaussian functions F(A) and F(B) are expressed by equation 9.

$$F(A) = \sum_i K_A i e^{-L} {}_{A,i} (R_{AB} - M_{A,i})^2$$
$$F(B) = \sum_i K_B i e^{-L} {}_{B,i} (R_{AB} - M_{B,i})^2$$

(9)

And finally AM1 core-repulsion function becomes (equation 10).

$$E_{AB}^{AM1} = E_{AB}^{MMDO}$$
$$+ \frac{Z_A Z_B}{R_{AB}} \left\{ \sum_i K_{A,i} e \left[-L_{A,i} (R_{AB} - M_{A,i})^2 \right] + \sum_j K_{B,j} e \left[-L_{B,j} (R_{AB} - M_{B,j})^2 \right] \right\}$$

(10)

In this equation 10, K, L and M are the Gaussian parameters. The remaining parameters have the same meaning as in the previous section. L parameters determine the widths of the Gaussians and were not found to be critical by Dewar. Therefore, a common value was used for many of the L parameters. On the other hand, all K and M parameters were optimized. Each atom has up to four of the Gaussian parameters, i.e., K1, …, K4, L1, …, L4, M1, …, M4. Carbon has four terms in its Gaussian expansion whereas hydrogen and nitrogen have three and oxygen has two terms (only K1, K2, L1, L2, M1, M2). Because in AM1 for carbon, hydrogen and nitrogen both attractive and repulsive Gaussians were used whereas for oxygen only repulsive ones considered, addition of Gaussian functions into the core-repulsion function significantly increased the number of parameters to be optimized and made the parameterization process more difficult. As for original MNDO, one-center two-electron repulsion integrals *gss*, *gpp*, *gdd*, *gsp*, *hsp* are assigned to atomic spectral values and not optimized. In contrast to MNDO, in which parameters were first optimized for carbon and hydrogen together and then other elements added one at a time, by increased computer resources and improved optimization procedure a larger reference parameterization dataset was used in the parameterization of AM1. All the parameters for H, C, N and O were optimized at once in a single parameterization procedure.

Optimization of the original AM1 elements was performed manually by Dewar using chemical knowledge and intuition. He also kept the size of the reference parameterization data at a minimum by very carefully selecting necessary data to be used as reference. Over the following years many of the main-group elements have been parameterized keeping the original AM1 parameters for H, C, N and O unchanged. Of course, a sequential parameterization scheme caused every new parameterization to depend on previous ones, which directly affects the quality of the results. AM1 represented

a very considerable improvement over MNDO without any increase in the computing time needed.

AM1 has been parameterized for many of the main-group elements and is very widely used, keeping its popularity in organic compounds' modeling due to its good performance and robustness. Although many of the deficiencies in MNDO were corrected in AM1, it still has some important limitations as outlined in the historical development section [12].

1.3.2 PM3 Method

In 1989, Stewart introduced PM3, which can be considered as a reparameterization of AM1. This method was named as parametric method 3, considering MNDO and AM1 as the methods 1 and 2, respectively, as one of the three NDDO-based methods. In both MNDO and AM1, one-center electron repulsion integrals (gij, hij), which are five parameters *gss*, *gsp*, *gpp*, *gp2*, and *gsp*, are assigned values determined from atomic spectra by Oleari. PM3 differs from MNDO and AM1 and these one-center electron integrals are taken as parameters to be optimized.

PM3 also differs from AM1 in the number of Gaussian terms used in the core repulsion function. PM3 uses only two Gaussian terms per atom instead of up to four used by AM1. Another difference is that PM3 uses an automated parameterization procedure, in contrast to AM1. H, C, N, O, F, Al, Si, P, S, Cl, Br, and I parameters were simultaneously parameterized, whereas AM1 parameters were adjusted manually by Dewar with the help of chemical knowledge or intuition. Since his parameter optimization algorithms permitted an efficient search of parameter space, Stewart was able to employ a significantly larger data set in evaluating his penalty function than had been true for previous efforts. Statistically, PM3 was more accurate than the other semiempirical methods available at the time, but it was found to have several deficiencies that seriously limited its usefulness. One of the most important of these is the rotational barrier of the amide bond, which is much too low and in some cases almost non-existent. The other one is that PM3 has a very strong tendency to make the environment around nitrogen pyramidal. Thus, PM3 is not suggested for use in studies where the state of hybridization of nitrogen is important. According to a search of "Current Contents" done in 1999, AM1 was the most widely used semiempirical quantum mechanical method and PM3 was second [12].

Theory

Both MNDO and AM1 had been parameterized by hand with the help of chemical knowledge and intuition using few reference data. Stewart had a more mathematical philosophy for the parameterization procedure and thought automated search of parameter space using complex optimization algorithm might be more successful to obtain better parameters. He made an optimization process by deriving and implementing formulae for the derivative of a suitable error function with respect to the parameters (equation 11).

$$S = \sum_{I}\left(x_i^{calc} - x_i^{ref}\right)^2 \qquad (11)$$

Where *S* is defined as the sum of the squares of the differences between calculated or predicted (x_i^{calc}) and reference values (x_i^{ref}) for reference functions, the parameter set is modified to minimize the value of *S*, and parameters are considered as *optimized* when for a given set of parameters, the sum square of errors, *S*, is a minimum.

In PM3, for each of the element's parameter set consists of 18 parameters (*Uss*, *Upp*, β*s*, β*p*, ζ*p*, ζ*s*, α, *gss*, *gpp*, *gsp*, *gp2*, *hsp*, *K1, K2, L1, L2, M1, M2*) except for hydrogen, which has 11 parameters only since parameters related to *p*-orbitals are not included.

As different from MNDO and AM1, in PM3 the one-center electron repulsion parameters are (*gij*, *hij*) optimized instead of assigning to atomic spectral values. PM3 also shares the same core-repulsion function with AM1 which is given as equation 12.

$$\begin{aligned} E_{AB}^{PM3} = E_{AB}^{MMDO} \\ + \frac{Z_A Z_B}{R_{AB}}\left\{\sum_i K_{A,i}e\left[-L_{A,i}(R_{AB}-M_{A,i})^2\right] + \sum_j K_{B,j}e\left[-L_{B,j}(R_{AB}-M_{B,j})^2\right]\right\} \end{aligned} \qquad (12)$$

But it uses only two Gaussian terms ($i = 1, 2$ and $j = 1, 2$ above) for each atom instead of four in AM1 ($i = 1,...,4$ and $j = 1,…,4$).

In the initial parameterization of PM3, twelve elements (H, C, N, O, F, Al, Si, P, S, Cl, Br and I) were optimized simultaneously and then following parameterizations were carried out keeping the parameters for these elements fixed. PM3 may have global minimum in comparing with MNDO and AM1, but this global minimum is obtained for a specific penalty function used and it is heavily affected by the type of compounds included in the parameterization

dataset. Thus, it does not necessarily supersede MNDO and AM1 especially for any particular type of problem [12].

The combination of quantum mechanics and molecular mechanics is a natural approach for the study of materials science. The active site or binding site is treated by the *ab initio* density functional theory or semi-empirical potentials, whereas the rest of the system is calculated by the force fields based on molecular mechanics. In the current version of *sander*, one can use the MNDO, AM1, or PM3 semi-empirical Hamiltonian for the quantum mechanical region. Interaction between the QM and MM regions includes electrostatics (based on partial charges in the MM part) and Lennard–Jones terms, designed to mimic the exchange-repulsion terms that keep QM and MM atoms from overlapping [13].

1.4 Gibbs Energy Free

In thermodynamics, the Gibbs free energy is a thermodynamic potential that measures the "useful" or process-initiating work obtainable from a thermodynamic system at a constant temperature and pressure (isothermal, isobaric). Just as in mechanics, where potential energy is defined as capacity to do work, similarly different potentials have different meanings. The Gibbs free energy is the *maximum* amount of non-expansion work that can be extracted from a closed system; this maximum can be attained only in a completely reversible process. When a system changes from a well-defined initial state to a well-defined final state, the Gibbs free energy ΔG equals the work exchanged by the system with its surroundings, minus the work of the pressure forces, during a reversible transformation of the system from the same initial state to the same final state.

Gibbs energy (also referred to as ΔG) is also the chemical potential that is minimized when a system reaches equilibrium at constant pressure and temperature. Its derivative with respect to the reaction coordinate of the system vanishes at the equilibrium point. As such, it is a convenient criterion of spontaneity for processes with constant pressure and temperature. The Gibbs free energy is defined as (equation 13).

$$G(p,T) = U + pV - TS \tag{13}$$

Which is the same as (equation 14).

$$G(p,T) = H - TS \tag{14}$$

Where:

U is the internal energy (SI unit: joule).

p is pressure (SI unit: pascal).

V is volume (SI unit: m^3).

T is the temperature (SI unit: kelvin).

S is the entropy (SI unit: joule per kelvin).

H is the enthalpy (SI unit: joule).

The expression for the infinitesimal reversible change in the Gibbs free energy as a function of its 'natural variables' p and T, for an open system, subjected to the operation of external forces (for instance electrical or magnetical) X_i, which cause the external parameters of the system a_i to change by an amount da_i, can be derived as follows from the First Law for reversible processes (equation 15).

$$TdS = dU + pdV - \sum_{i=1}^{K} \mu_i dN_i + \sum_{i=1}^{n} X_i da_i + ...$$

$$d(TS) - SdT - dU + d(pV) - Vdp - \sum_{i=1}^{K} \mu_i dN_i + \sum_{i=1}^{n} X_i da_i + ...$$

$$d(U - TS + pV) - Vdp - SdT + \sum_{i=1}^{K} \mu_i dN_i + \sum_{i=1}^{n} X_i da_i + ...$$

$$dG - Vdp - SdT + \sum_{i=1}^{K} \mu_i dN_i + \sum_{i=1}^{n} X_i da_i + ...$$

(15)

Where:

- μ_i is the chemical potential of the ith chemical component. (SI unit: joules per particle or joules per mole.)
- N_i is the number of particles (or number of moles) composing the ith chemical component.

This is one form of Gibbs fundamental equation. In the infinitesimal expression, the term involving the chemical potential accounts for changes in Gibbs free energy resulting from an influx or out flux of particles. In other words, it holds for an open system. For a closed system, this term may be dropped. Let the change ΔG in Gibbs free energy be defined as equation 16.

$$\Delta G = \Delta H - T\Delta S_{int} \tag{16}$$

Notice that it is not defined in terms of any external state functions, such as ΔS_{ext} or ΔS_{tot}. Then the second law becomes, which also tells us about the spontaneity of the reaction.

$\Delta G < 0$ Favoured reaction (Spontaneous)

$\Delta G = 0$ Neither the forward nor the reverse reaction prevails (Equilibrium)

$\Delta G > 0$ Disfavoured reaction (Nonspontaneous)

Gibbs free energy *G* itself is defined as equation 17.

$$G = H - TS_{int} \tag{17}$$

But notice that to obtain equation (17) from equation (16) we must assume that *T* is constant. Thus, Gibbs free energy is most useful for thermochemical processes at constant temperature and pressure: both isothermal and isobaric. Such processes don't move on a *P-V* diagram, such as phase change of a pure substance, which takes place at the saturation pressure and temperature. Chemical reactions, however, do undergo changes in chemical potential, which is a state function. Thus, thermodynamic processes are not confined to the two dimensional *P-V* diagram. There is a third dimension for *n*, the quantity of gas. For the study of explosive chemicals, the processes are not necessarily isothermal and isobaric. For these studies, Helmholtz free energy is used. If an isolated system ($Q = 0$) is at constant pressure ($Q = \Delta H$), then

$$\Delta H = 0 \tag{18}$$

Therefore the Gibbs free energy of an isolated system is:

$$\Delta G = T\Delta S_{int} \tag{19}$$

And if $\Delta G \leq 0$ then this implies that $\Delta S \geq 0$, back to where we started the derivation of ΔG [14-15].

1.5 Electrostatic Potential

The electrostatic force is a conservative force. This means that the work it does on a particle depends only on the initial and final position of the particle and not on the path followed. With each conservative force, a potential energy can be associated. The introduction of the potential energy is useful since it

allows us to apply conservation of mechanical energy which simplifies the solution of a large number of problems. The potential energy U associated with a conservative force F is defined in the following manner (equation 20).

$$U(P_1) - U(P_0) = -W = \int_{P_0}^{P_1} \bar{F} \ d\bar{L} \tag{20}$$

Where $U(P_0)$ is the potential energy at the reference position P_0 (usually $U(P_0)$ = 0) and the path integral is along any convenient path connecting P_0 and P_1. Since the force F is conservative, the integral in eq.(25.1) will not depend on the path chosen. If the work W is positive (force and displacement pointing in the same direction) the potential energy at P_1 will be smaller than the potential energy at P_0. If energy is conserved, a decrease in the potential energy will result in an increase of the kinetic energy. If the work W is negative (force and displacement pointing in opposite directions) the potential energy at P_1 will be larger than the potential energy at P_0. If energy is conserved, an increase in the potential energy will result in a decrease of the kinetic energy. If In electrostatic problems the reference point P_0 is usually chosen to correspond to an infinite distance and the potential energy at this reference point is taken to be equal to zero. Equation (25.1) can then be rewritten as:

$$U_c(P_1) = -\int_{P_0}^{P_1} \bar{F}_c \ d\bar{L} \tag{21}$$

To describe the potential energy associated with a charge distribution the concept of the electrostatic potential V is introduced. The electrostatic potential V at a given position is defined as the potential energy of a test particle divided by the charge q of this object:

$$\begin{aligned} V_c(P_1) = \frac{U_c(P_1)}{q} &= \frac{U_c(P_0)}{q} - \frac{1}{q}\int_{P_0}^{P_1} \bar{F}_c \ d\bar{L} \\ &= V_c(P_0) - \frac{1}{q}\int_{P_0}^{P_1} \bar{F}_c \ d\bar{L} \\ &= -\frac{1}{q}\int_{P_0}^{P_1} \bar{F}_c \ d\bar{L} \end{aligned} \tag{22}$$

In the last step of equation (22) we have assumed that the reference point P_0 is taken at infinity, and that the electrostatic potential at that point is equal to 0. Since the force per unit charge is the electric field, equation (23) can be rewritten as:

$$V_c(P_1) = -\int_{P_0}^{P_1} \overline{E} \, d\overline{L} \qquad (23)$$

The unit of electrostatic potential is the volt (V), and $V = J/C = Nm/C$. Equation (23) shows that as the unit of the electric field we can also use V/m.

A common used unit for the energy of a particle is the electron-volt (eV) which is defined as the change in kinetic energy of an electron that travels over a potential difference of 1 V. The electron-volt can be related to the Joule via eq.(23). Equation (23) shows that the change in energy of an electron when it crosses over a 1V potential difference is equal to 1.6×10^{-19} J and we thus conclude that $1 \text{ eV} = 1.6 \times 10^{-19}$ J.

In many electrostatic problems the electric field of a certain charge distribution must be evaluated. The calculation of the electric field can be carried out using two different methods:

1. The electric field can be calculated by applying Coulomb's law and vector addition of the contributions from all charges of the charge distribution.
2. The total electrostatic potential V can be obtained from the algebraic sum of the potential due to all charges that make up the charge distribution, and subsequently using equation (23) to calculate the electric field E.

In many cases method 2 is simpler since the calculation of the electrostatic potential involves an algebraic sum, while method 1 relies on the vector sum [16].

1.6 Molecular Orbitals

A molecular orbital (or MO) is a mathematical function describing the wave-like behavior of an electron in a molecule.

This function can be used to calculate chemical and physical properties such as the probability of finding an electron in any specific region. Molecular orbitals (MOs) represent regions in a molecule where an electron is likely to be

found. Molecular orbitals are obtained from the combination of atomic orbitals, which predict the location of an electron in an atom.

A molecular orbital can specify the electron configuration of a molecule: the spatial distribution and energy of one (or one pair of) electron(s). Most commonly an MO is represented as a linear combination of atomic orbitals (the LCAO-MO method), especially in qualitative or very approximate usage. They are invaluable in providing a simple model of bonding in molecules, understood through molecular orbital theory. Most present-day methods in computational chemistry begin by calculating the MOs of the system.

A molecular orbital describes the behavior of one electron in the electric field generated by the nuclei and some average distribution of the other electrons. In the case of two electrons occupying the same orbital, the Pauli principle demands that they have opposite spin. Necessarily this is an approximation, and highly accurate descriptions of the molecular electronic wave function do not have orbitals (see configuration interaction). Molecular orbitals arise from allowed interactions between atomic orbitals, which are allowed if the symmetries (determined from group theory) of the atomic orbitals are compatible with each other.

Efficiency of atomic orbital interactions is determined from the overlap (a measure of how well two orbitals constructively interact with one another) between two atomic orbitals, which is significant if the atomic orbitals are close in energy. Finally, the number of molecular orbitals that form must equal the number of atomic orbitals in the atoms being combined to form the molecule. The type of interaction between atomic orbitals can be further categorized by the molecular-orbital symmetry labels σ (sigma), π (pi), etc. paralleling the symmetry of the atomic orbitals s, p, etc.

σ Symmetry. A MO with σ symmetry results from the interaction of either two atomic s-orbitals or two atomic p_z-orbitals. A MO will have σ-symmetry if the orbital is symmetrical with respect to the axis joining the two nuclear centers, the internuclear axis. This means that rotation of the MO about the internuclear axis does not result in a phase change. A σ* orbital, sigma antibonding orbital, also maintains the same phase when rotated about the internuclear axis. The σ* orbital has a nodal plane that is between the nuclei and perpendicular to the internuclear axis.

δ Symmetry. A MO with δ symmetry results from the interaction of two atomic d_{xy} or $d_{x^2-y^2}$ orbitals. Because these molecular orbitals involve low-

energy d atomic orbitals, they are seen in transition-metal complexes.

π Symmetry. A MO with π symmetry results from the interaction of either two atomic p_x orbitals or p_y orbitals. A MO will have π symmetry if the orbital is asymmetrical with respect to rotation about the internuclear axis. This means that rotation of the MO about the internuclear axis will result in a phase change. A π* orbital, pi antibonding orbital, will also produce a phase change when rotated about the internuclear axis. The π* orbital also has a nodal plane between the nuclei.

φ Symmetry. Theoretical chemists have conjectured that higher-order bonds, such as phi bonds corresponding to overlap of "f atomic orbitals", are possible. There is as of 2005 only one known example of a molecule purported to contain a phi bond (a U−U bond, in the molecule U_2) (Figure 1.10) [17-18].
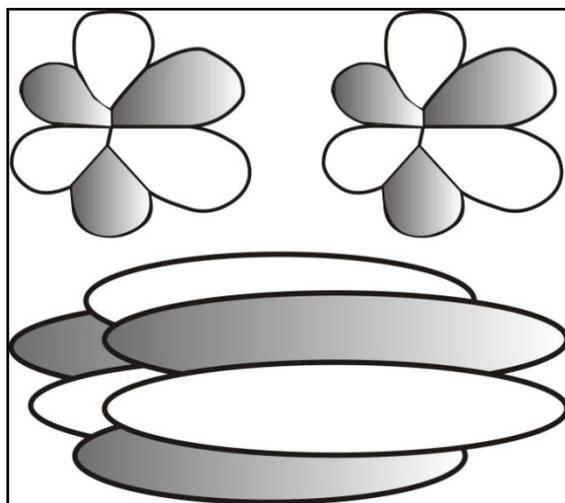
Figure 1.10 *Suitably aligned f atomic orbitals overlap to form phi molecular orbital (a phi bond).*

When we are dealing with interacting molecular orbitals, the two that interact are generally:

- The highest energy occupied molecular orbital (HOMO) of one molecule.
- The lowest energy unoccupied molecular orbital (LUMO) of the other molecule.
- These orbitals are the pair that lie closest in energy of any pair of orbitals in the two molecules, which allows them to interact most strongly.

- These orbitals are sometimes called the *frontier* orbitals, because they lie at the outermost boundaries of the electrons of the molecules (Figure 1.11) [19].
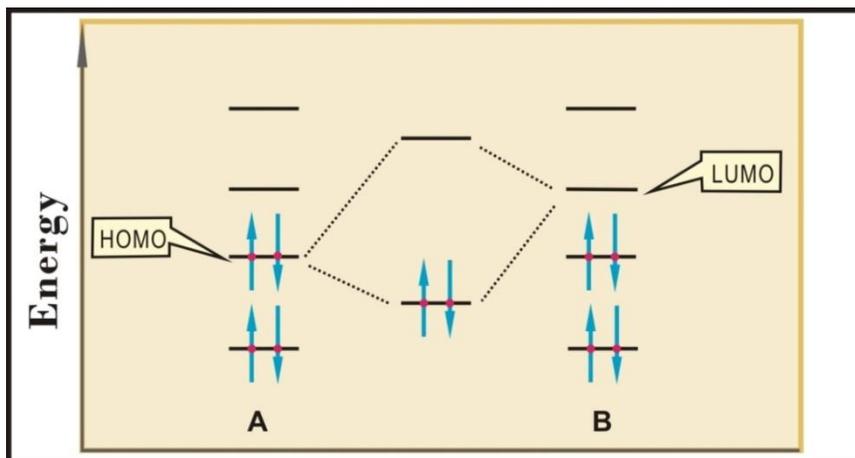
Figure 1.11 *Filled-empty interactions redrawn as a HOMO-LUMO interaction.*

References

[1]   Salih S M. AM1 semi-empirical calculation to study the nature of di- and tri-molecular assembly of π, π-aromatic interactions. *The Arabian Journal for Science and Engineering,* 35 (2A), 95-113, 2010.

[2]   www.tau.ac.il/~ephraim/MM+MD.doc.

[3]   Cornell W D, Cieplak P, Bayly C I, Gould I R, Merz K M Jr, Ferguson D M, Spellmeyer D C, Fox T, Caldwell J W, Kollman P A. A Second Generation Force Field for the Simulation of Proteins, Nucleic Acids, and Organic Molecules. *J. Am. Chem. Soc.* 117: 5179–5197, 1995.

[4]   Abdulsattar M A, Al-Bayati K H. Corrections and parameterization of semiempirical large unit cell method for covalent semiconductors. *Phys. Rev. B.* 75, 245201, 2007.

[5]   Abdulsattar M A. Size effects of semiempirical large unit cell method in comparison with nanoclusters properties of diamond-structured covalent semiconductors, *Physica E.* 41, 1679, 2009.

[6]   Levine I. *Quantum Chemistry*, Prentice Hall, 4th edition, 579–580, 1991.

[7]   Cramer C J. Essentials of Computational Chemistry. *Wiley*, Chichester, 126–131, 2002.

[8]   Stewart J. J. P. Reviews in Computational Chemistry, Volume 1, Eds. K. B. Lipkowitz and D. B. Boyd, VCH, New York, 45, 1990.

[9]   Rocha G B, Freire R O, Simas A M, Stewart J J P. RM1: A reparameterization of AM1 for H, C, N, O, P, S, F, Cl, Br, and I. *The Journal of Computational Chemistry.* 27(10), 1101–1111, 2006.

[10]   Stewart J J P. Optimization of Parameters for Semiempirical Methods V: Modification of NDDO Approximations and Application to 70 Elements. *The Journal of Molecular Modeling.* 13(12), 1173–1213, 2007.

[11]   Zerner M, Reviews in Computational Chemistry, Volume 2, Eds. K. B. Lipkowitz and D. B. Boyd, VCH, New York, 313, 1991.

[12]   B änsch E, Clark T, Burzlaff N. Parameterization of the am1* semiempirical molecular orbital method for the first-row transition metals and other elements, Turqu á, 2009.

[13]   Ryde U. Combined quantum and molecular mechanics calculations on metalloproteins. *Curr Opin Chem Biol*. 7, 136-142, 2003.

[14]   Salzman W R. *Chemical Thermodynamics*. University of Arizona, 2001. http://web.archive.org/web/20070707224025/http://www.chem.arizona.edu/~salz manr/480a/480ants/opensys/opensys.html.

[15]   CRC Handbook of Chemistry and Physics, 2009, pp. 5-4 - 5-42, 90th ed., Lide M üller, Ingo (2007). *A History of Thermodynamics - the Doctrine of Energy and Entropy*. Springer. ISBN 978-3-540-46226-2.

[16]   http://teacher.nsrl.rochester.edu/phy122/Lecture_Notes/Chapter25/Chapter25.html.

[17]   Atkins P. Atkins J P. Physical Chemistry. *Oxford University Press*, 8th ed., 2006.

[18]   Gary L. Miessler; Donald A. Tarr. Inorganic Chemistry. Pearson Prentice Hall, 3rd ed., 2004.

[19]   Department of Chemistry, University of Maine, Orono, ME 04469 (http://chemistry.umeche.maine.edu/CHY252/HOMO-LUMO.html).

Chapter 2

Methodology

Chapter 2

Methodology

NORMA AUREA RANGEL-VÁZQUEZ[1]
FRANCISCO RODRÍGUEZ FÉLIX[2]

[1]División de Estudios de Posgrado e Investigación del Instituto Tecnológico de Aguascalientes, Ave. López Mateos # 1801 Ote. Fracc. Bona Gens CP. 20256 Aguascalientes, Aguascalientes, México
[2]Departamento de Investigación y Posgrado en Alimentos. Universidad de Sonora, Blvd. Luis Encinas y Rosales S/N Col. Centro, Hermosillo, Sonora, México

Abstract

Conditions for simulations using the PM3 and AM1 methods were established in this chapter. The simulations allow determining the reaction conditions of different materials, so through the application of methods PM3 and AM1 were determined Gibbs free energy. In addition the main signals of vibrational and sites for nucleophilic and electrophilic attacks of different structures simulated.

Keywords: FTIR, Electrostatic Potential, Structural Parameters

2.1 Geometry Optimization

It is necessary to carry out the geometry optimization or energy minimization of the system being examined. After it has been sketched, since sketching often creates the structure in a high energy configuration and starting a simulation from such an unoptimized structure can lead to erroneous simulations and results. In this work three aspects were considered to selection of geometry optimization method and algorithm: system size, convergence level and force field used. In this study the semi-empirical methods were used for describing the potential energy function of the system. Next a minimization algorithm is chosen to find the potential energy minimum corresponding to the lower-energy

structure. Iterations number and convergence level lead optimal structure. The optimizing process of structures used in this work was started using the PM3 and AM1 methods, because it generates a lower-energy structure even when the initial structure is far away from the minimum structure. The Polak-Ribiere algorithm was used for mapping the energy barriers of the conformational transitions. For each structure, 1350 iterations, a level convergence of 0.001 kcal/mol/Å and a line search of 0.1 were carried out [1].

2.2 Structural Parameters

The optimized structural parameters were used in the vibrational wavenumber calculation with PM3 and AM1 method to characterize all stationary points as minima. The structural parameters were calculated select the Constrain bond and length options of Build menu for two method of analysis.

2.3 FTIR

The infrared spectrum is commonly obtained by passing infrared electromagnetic radiation through a sample that possesses a permanent or induced dipole moment and determining what fraction of the incident radiation is absorbed at a particular energy [2]. The energy of each peak in an absorption spectrum corresponds to the frequency of the vibration of a molecule part, thus allowing qualitative identification of certain bond types in the sample.

The FTIR was obtained by first selecting menu Compute, vibrational, rotational option, once completed this analysis, using the option vibrational spectrum of FTIR spectrum pattern is obtained for two methods of analysis.

2.4 Electrostatic Potential

After obtaining a free energy of Gibbs or optimization geometry using PM3 and AM1 methods, we can plot two-dimensional contour diagrams of the electrostatic potential surrounding a molecule, the total electronic density, the spin density, one or more molecular orbitals, and the electron densities of individual orbitals.

HyperChem software displays the electrostatic potential as a contour plot

when you select the appropriate option in the Contour Plot dialog box. Choose the values for the starting contour and the contour increment so that you can observe the minimum (typically about –0.5 for polar organic molecules) and so that the zero potential line appears.

A menu plot molecular graph, the electrostatic potential property is selected and then the 3D representation mapped isosurface for both methods of analysis. Atomic charges indicate where large negative values (sites for electrophilic attack) are likely to occur. However, the largest negative value of the electrostatic potential is not necessarily adjacent to the atom with the largest negative charge [3].

2.5 Orbitals Molecular

The interaction between charges favors reaction between sites (on the two species) that have extreme charge values: the most positive charge interacts with the most negative. This ionic reaction generally involves strongly polar reactants. The second term favors interactions where the HOMO and the LUMO can overlap most favorably. This generally occurs for less polar reactants and is important when the two have similar energies, so that the denominator is small [3].

The HOMO–LUMO analysis has been carried out to explain the charge transfer within the molecule. The chemical hardness (g) and chemical potential (l) have been calculated using the highest occupied molecular orbital (HOMO) and lowest unoccupied molecular orbital (LUMO). This analysis has been performed using PM3 and AM1 method level in order to elucidate the intermolecular hydrogen bonding, intermolecular charge transfer (ICT), rehybridization, and delocalization of electron density [4].

2.6 Conclusions

Conditions for simulations using the PM3 and AM1 methods were established in this chapter. Geometry optimization was determined to obtain the Gibbs free energy and determinate the spontaneity of the reaction. The structural parameters are calculated to indicate whether the molecules is linear or not, by the length and angle bond. With FTIR analyses the characteristic signals were calculated. Finally, the analysis of molecular orbital and electrostatic potentials were obtained to assigned where the attractions will be

stronger to form bonds.

References

[1] López-Chávez E, Oviedo-Roa R, Contreras-Pérez G, Martínez-Magadán J M, Castillo-Alvarado F L, Theoretical studies of ionic conductivity of crosslinked chitosan membranes, *International Journal of Hydrogen Energy*, 35(21), 12141–12146, 2010.

[2] Kumirska J, Czerwicka M, Kaczyński Z, Bychowska A, Brzozowski K, Thöming J, Stepnowski P. Application of Spectroscopic Methods for Structural Analysis of Chitin and Chitosan, *Mar Drugs*. 8(5), 1567–1636, 2010.

[3] HyperChem® Computational Chemistry, Canada, 1996.

[4] Gayathri R, Arivazhagan M. Experimental (FT-IR and FT-Raman) and theoretical (HF and DFT) investigation, NMR, NBO, electronic properties and frequency estimation analyses on 2,4,5-trichlorobenzene sulfonyl chloride. *Spectrochimica Acta Part A: Molecular and Biomolecular Spectroscopy.* 97, 311–325, 2012.

Chapter 3

Chitosan

Chapter 3

Chitosan

NORMA AUREA RANGEL-VÁZQUEZ[1]
FRANCISCO RODRÍGUEZ FÉLIX[2]
BÁRBARA-SUSANA GREGORÍ VALDÉS[3]

[1]*División de Estudios de Posgrado e Investigación del Instituto Tecnológico de Aguascalientes, Ave. López Mateos # 1801 Ote. Fracc. Bona Gens CP. 20256 Aguascalientes, Aguascalientes, México*

[2]*Departamento de Investigación y Posgrado en Alimentos. Universidad de Sonora, Blvd. Luis Encinas y Rosales S/N Col. Centro, Hermosillo, Sonora, México*

[3]*Institute for Biotechnology and Bioengineering, Centre for Biological and Chemical Engineering, Instituto Superior Técnico, Av. Rovisco Pais 1, 1049-001 Lisboa, Portugal*

Abstract

Chitosan is a linear polysaccharide composed of randomly distributed β-(1-4)-linked D-glucosamine (deacetylated unit) and N-acetyl-D-glucosamine (acetylated unit). It is made by treating shrimp and other crustacean shells with the alkali sodium hydroxide. Chitosan has a number of commercial and possible biomedical uses. It can be used in agriculture as a seed treatment and biopesticide, helping plants to fight off fungal infections. In winemaking it can be used as a fining agent, also helping to prevent spoilage. In industry, it can be used in a self-healing polyurethane paint coating. In medicine, it may be useful in bandages to reduce bleeding and as an antibacterial agent; it can also be used to help deliver drugs through the skin.

Molecular modeling simulations are the most important tools to predict blend compatibility of polymers that are otherwise difficult to predict by experimental means. PM3 and AM1 *calculation is performed to obtain the Gibbs free energy, structural parameters, FTIR, molecular orbitals in chitosan.*

Keywords: Chitosan, Chitin, PM3, AM1, Simulation

3.1 Introduction

Among the novel families of biological macromolecules, whose relevance is becoming increasingly evident, are chitin and its main derivative, chitosan [1]. Potential and usual applications of chitin, chitosan and their derivatives are estimated to be more than 200. This wide range of applications includes biomedicine, food, biotechnology, agriculture and cosmetics, among others [1-2]. In addition to low cost, relative abundance, and biocompatibility, one of the appealing factors of using chitosan *in vivo* has been its wound healing properties [2].

Chitin and chitosan are described as a family of linear polysaccharides consisting of varying amounts of β (1→4) linked residues of N-acetyl-2 amino-2-deoxy-D-glucose (denoted in this review as A residues) and 2-amino-2-deoxy-Dglucose residues (denoted in this review as D residues). Chitin samples have a low amount of D units and hence the polymer is insoluble in acidic aqueous media (Figure 3.1).
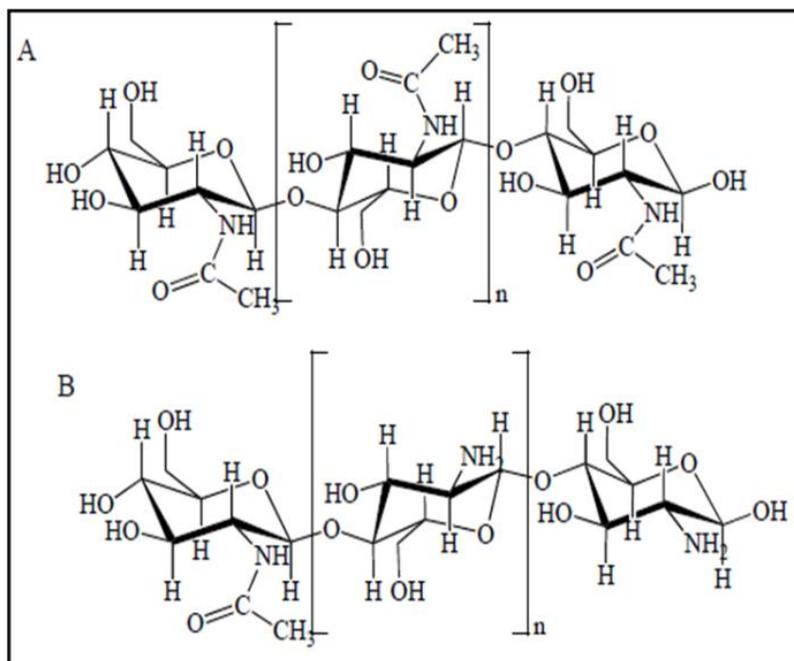
Figure 3.1 Chemical structure of 100% acetylated chitin (a) and chitosan (b).

On the other hand, the amount of D units in chitosan samples is high enough

to allow the polymer to dissolve in acidic aqueous media. Some authors consider that chitosan is the polymer with at least 60% of D residues. Chitin is the second most abundant natural polymer in nature after cellulose and it is found in the structure of a wide number of invertebrates (crustaceans' exoskeleton, insects' cuticles) and the cell walls of fungi, among others. On the other hand, chitosan only occurs naturally in some fungi (*Mucoraceae*) [1].

3.2 Synthesis

Chitosan is produced commercially by deacetylation of chitin, which is the structural element in the exoskeleton of crustaceans (such as crabs and shrimp) and cell walls of fungi. The degree of deacetylation (%DD) can be determined by NMR spectroscopy, and the %DD in commercial chitosans ranges from 60 to 100%. On average, the molecular weight of commercially produced chitosan is between 3800 and 20,000 Daltons. A common method for the synthesis of chitosan is the deacetylation of chitin using sodium hydroxide in excess as a reagent and water as a solvent. This reaction pathway, when allowed to go to completion (complete deacetylation) yields up to 98% product [3]. The amino group in chitosan has a pKa value of ~6.5, which leads to a protonation in acidic to neutral solution with a charge density dependent on pH and the %DA-value. This makes chitosan water soluble and a bioadhesive which readily binds to negatively charged surfaces such as mucosal membranes.

Chitosan enhances the transport of polar drugs across epithelial surfaces, and is biocompatible and biodegradable. Purified quantities of chitosans are available for biomedical applications. Chitosan and its derivatives, such as trimethylchitosan (where the amino group has been trimethylated), have been used in nonviral gene delivery. Trimethylchitosan, or quaternised chitosan, has been shown to transfect breast cancer cells, with increased degree of trimethylation increasing the cytotoxicity; at approximately 50% trimethylation, the derivative is the most efficient at gene delivery. Oligomeric derivatives (3-6 kDa) are relatively nontoxic and have good gene delivery properties [4].

3.3 Applications

The potential applications of modified chitosan in various important fields, such as environment, drug delivery, tissue engineering and other biomedical application are here discussed. An attempt is also made to discuss some of the current applications and future prospects of modified chitosan.

3.3.1 Drug Delivery

Chitosan has interesting biopharmaceutical characteristics such as pH sensitivity, biocompatibility and low toxicity. Moreover, chitosan is metabolised by certain human enzymes, especially lysozyme, and is biodegradable. Due to these favorable properties, the interest in chitosan and its derivatives in drug delivery applications have been increased in recent years. Moreover, in such applications it is also extremely important that chitosan be hydro-soluble and positively charged. These properties enable it to interact with negatively charged polymers, macromolecules and polyanions in an aqueous environment. Many works related with potential applications of chitosan and its derivatives can be found in literature. For instance, it has been shown that chitosan and its derivatives, such as *N*-trimethyl chitosan or *N*-carboxymethyl chitosan, have the special feature of adhering to mucosal surfaces, being useful for mucosal drug delivery.

Acrylic acid grafts of chitosan as possible means of creating hydrophilic and mucoadhesive polymers have been reported recently. Chitosan-grafted poly (acrylic acid) particles have been proposed as hydrophilic drug carriers for hydrophilic drugs and sensitive proteins. Kumbar et al. prepared microspheres of polyacrylamide-grafted-chitosan crosslinked with glutaraldehyde to encapsulate indomethacin (IM), a nonsteroidal anti-inflammatory drug used in the treatment of arthrhitis. Microspheres of grafted chitosan crosslinked with glutaraldehyde were prepared to encapsulate nifidifine (NFD), a calcium channel blocker and an antihypertensive drug.

N-Lauryl carboxymethyl chitosan with both hydrophobic and hydrophilic groups was studied in connection with the delivery of taxol to cancerous tissues. Other examples are related to the production of polymeric vesicles for encapsulation of hydrophobic compounds like bleomycin.

Some works related with intracellular delivery for gene therapy using modified chitosan-based materials were reported. In fact it has been argued that the most important application of alkylated chitosan is in DNA delivery such as proven with dodecyl chitosan. The high transfection efficiency of alkylated chitosan was attributed to the increasing entry into cells facilitated by hydrophobic interactions and easier unpacking of DNA from alkylated chitosan carriers, due to the weakening of electrostatic attractions between DNA and alkylated chitosan.

In another work, deoxycholic acid, which is the main component of bile acids,

was used to modify chitosan hydrophobically and to obtain self-assembling macromolecules for non-viral gene delivery system. The self-aggregate DNA complex from deoxycholic acid-modified chitosan was shown to enhance the transfection efficiency over monkey kidney cells. The feasibility of these chitosan self-aggregates for the transfection of genetic material in mammalian cells was investigated. Self-aggregates can form charge complexes when mixed with plasmid DNA. These self-aggregate DNA complexes are considered to be useful for transfer of genes into mammalian cells *in vitro* and served as good delivery system composed of biodegradable polymeric materials. PEGylation of chitosan in order to increase its solubility, elongate the plasma circulation time and prolong the gene transfer has been another proposed technique for the sustained DNA release. For example, Zhang et al prepared chitosan–DNA complexes conjugated with alpha methoxy-omega-succinimidyl PEG, and the gene expression was improved in comparison with the chitosan–DNA complex both *in vitro* and *in vivo*. Microspheres physically combining PEG-grafted chitosan (PEG-*g*-CHI) with poly (lactide-co-glycolide) (PLGA) were formulated by Yun et al. They reported that these microspheres were capable of sustained release of PEG-*g*-CHI/DNA for at least 9 weeks, and the rate of DNA release was not modulated by varying the amount of PEG-*g*-CHI.

In another work folate-PEG-grafted chitosan was synthesized and proposed for targeted plasmid DNA delivery to tumor cells. The authors found that folate conjugation in this system significantly improved gene transfection efficiency due to promoted uptake of folate receptor bearing tumor cells. *In vitro* and *in vivo* studies of gene transfection are being conducted in the laboratory to evaluate its gene transfection efficiency.

Very recently novel water-soluble nanoparticles that consist of a PAMAM dendrimer core with grafted carboxymethyl chitosan chains were successfully synthesized. The non-cytotoxicity and successful internalization of these dendrimer nanoparticles by two different types of cells, i.e., cell lines and primary cultures, was demonstrated in this work. The authors also showed that the dexamethasone-loaded nanoparticles induced the osteogenic differentiation of rat bone marrow stem cells *in vitro*. So, these novel dendrimer nanoparticles may be used as targeted drug-delivery carriers to cover a wide range of applications that involve the efficient intracellular delivery of biological agents to modulate the behaviour of cells.

Thiol-containing chitosan beads were synthesized in order to be used as a controlled and pH-responsive drug delivery system. It has been shown that P-chitosan beads have a great potential to be used as controlled drug release

systems through oral administration since the release in the highly acidic gastric fluid region of the stomach is avoided. Chitosan-based systems bearing β-cyclodextrin cavities have been proposed as a matrix for controlled release. Due to the presence of the hydrophobic β-cyclodextrin rings, these systems provide a slower release of the entrapped hydrophobic drug.

Finally, stimuli-responsive hydrogels have shown an improved drug loading capacity, and a sustained release behavior. In particular, systems that combine chitosan and PNIPAAm have shown drug release profiles that can be controlled by both pH and temperature, constituting very promising materials. This kind of smart systems has also been proposed for gene delivery. For instance, Sun et al. coupled a carboxyl-terminated NIPAAm/vinyl laurate (VL) copolymer with chitosan (PNVLCS) and examined the gene expression of PNVLCS/DNA complexes in C2C12 cells against temperature change.

The results indicated that the transfection efficiency of PNVLCS/DNA complexes was improved by dissociation of the gene from the carrier by temporarily reducing the culture temperature to 20 ℃. By contrast, naked DNA and lipofectamine did not demonstrate thermo-responsive gene transfection.

3.3.2 Tissue Engineering

The present generation of tissue engineering (TE) research is based on the seeding of cells onto porous biodegradable polymer matrixes. A primary factor is the availability of good biomaterials to serve as the temporary matrix. Recently, chitosan and its derivatives have been reported as attractive candidates for scaffolding materials because they degrade as the new tissues are formed, eventually without inflammatory reactions or toxic degradation. In TE applications the cationic nature of chitosan is primarily responsible for electrostatic interactions with anionic glycosaminoglycans, proteoglycans and other negatively charged molecules.

Some research works where the biological properties of chitosan and the mechanical properties of PLLA are combined have been reported. The *in vitro* fibroblast static cultivation on chitosan-grafted PLLA films for 11 days showed that the cell growth rate on these films was faster than in chitosan and decreased when the feed ratio of PLLA to chitosan increases. Surface functionalization of biodegradable PLLA was achieved by plasma coupling reaction of chitosan with PLLA.

The proliferation and morphology studies of two cell lines, L-929 (mouse fibroblasts) and L-02 (human hepatocytes), cultured on this surface showed that

cells hardly spread and tended to become round, but could proliferate at almost the same speed as cells cultured on glass surface. This insight will help to clarify the mechanism of the switch between cell growth and differentiation. This grafted polymer can be used to control themorphology and function of cells, and hence has potential applications in tissue engineering.

Very recently novel PLLA–chitosan hybrid scaffolds were proposed as tissue engineering scaffolds and simultaneously drug release carriers. In this innovative system a chitosan porous structure, in which cells and tissues would mostly interact, is created within the pore structure of a stiffer PLLA scaffold. It has been shown that thiolated chitosan can provide an adequate scaffold structure: due to the *in situ* gelling properties it seems possible to provide a certain shape of the scaffold material by pouring a liquid thiolated chitosan cell suspension in a mold.

Furthermore, liquid polymer cell suspensions may be applied by injection forming semi-solid scaffolds at the site of tissue damage. So they seem to be promising candidates for such applications. Surfaces that can induce the formation of an apatite layer *in vitro* demonstrate improved bone-binding properties and calcium phosphate growth on P-chitin fibers and P-chitosan films has been reported after soaking with Ca(OH)2.Water-soluble P-chitosans have been mixed with different calcium phosphate cements, showing an improvement in their properties, namely the mechanical strength, setting time, dissolubility of the start materials of the cements and they also bind calcium phosphate strongly afterwards. Moreover it has been shown that due to the smart nature of chitosan, the apatite formation of chitosan-grafted PLLA films reinforced with Bioglass® can be controlled by pH, which could also have relevance in bone TE applications [5].

Another approach regarding the chemical modification of chitosan for TE applications has been to introduce the specific recognition of cells by sugars. A recent example of the synthesis of sugar-bound chitosan can be found in the work of Kim et al.

They prepared mannosylated chitosan (MC) having the specific recognition to antigen presenting cells such as B-cells, dendritic cells and macrophages. In addition to applications in controlled drug release, PNIPAAmgrafted chitosan-based materials have been exploited for controlling cell adhesion/detachment by changing the incubation temperature above or below its LCST. Temperature responsive chitosan-graft-PNIPAAm was applied for the culture of mesenchymal stem cells (MSCs). Chitosan-*g*-PNIPAAm copolymers with

chondrogenic MSCs revealed the possibility of clinical applications, particularly as cell therapy technologies for treating vesicoureteral reflux [5].

3.4 Results and Discussion of Simulations Analyses

3.4.1 Optimization Energy

Table 3.1 shows the Gibbs free energy of the chitosan using different methods, in where the strong negative Gibbs free energy (ΔG) (see Table 3.1) calculated from the different methods shows that the electrostatic binding of chitosan is energetically favorable [6-7]. Attractive interactions between π systems are one of the principal non-covalent forces governing molecular recognition and play important roles in many chemical systems. Attractive interaction between π systems is the interaction between two or more molecules leading to self-organization by formation of a complex structure which has lower conformation equilibrium than of the separate components and shows different geometrical arrangement with high percentage of yield (Figure 3.2) [8]. It is evident from the reactional profiles that chitosan provides an abundance of reactive functional groups such as $-COO-$, $-NH_3^+$, $-OH$, $-CONH_2$, and $-NH_2$. The presence of such ionic functional groups may further provide a conductive surface environment for the growth and proliferation of the neural architecture on account of their mixed hydrophillicity/hydrophobicity and varied surface-to-charge ratio [9-10].

Table 3.1 *Gibbs energy free for chitosan structure.*

Method	ΔG (Kcal/mol)
AM1	-2273
PM3	-1966

3.4.2 Structural Parameters

Chitosan conformational diversity influences its solubility/physical state (soluble, gel, aggregate), porosity, particle size and shape (fiber, nanoparticle), ability to chelate metal ions and organic compounds, biodegradability and consequently its biological activity. The transition between these distinct conformational states is modulated by the percentage and distribution of acetyl groups. The level of chitosan acetylation and the distribution of N-acetyl groups along the chain have been shown to influence properties such as solubility, biodegradability and apparent pK_a values. Therefore, the percentage and

distribution of acetyl groups are key parameters for determining if chitosan can effectively interact with biological systems. The degree of acetylation can be experimentally determined by infra-red spectroscopy, ultra-violet spectroscopy and solid-state ^{13}C NMR. However, the interplay between chitosan acetylation and conformational transitions in solution cannot be characterized at high-resolution by experimental techniques. In these cases, the simulations are a more suitable approach [11]. The first task for a computational work was to determine the optimized geometry of chitosan. The molecular structure along with numbering of atoms of chitosan is as shown in Figure 3.2.
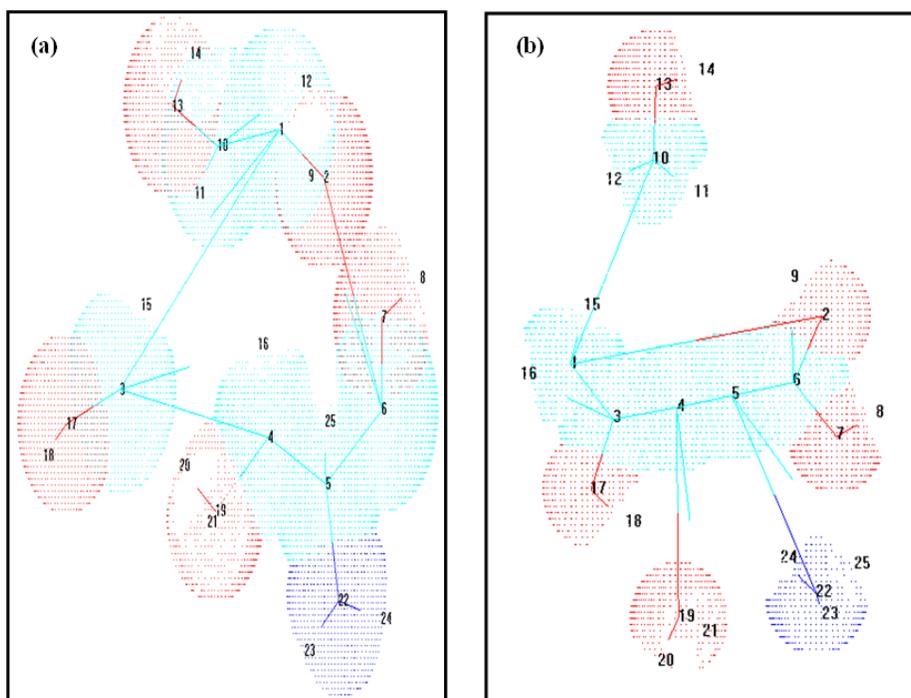
Figure 3.2 *Molecular geometry of chitosan, in where (a) PM3 and (b) AM1 method, respectively.*

The optimized structure parameter of chitosan calculated PM3 and AM1, is listed in Table 3.2 in accordance with the atom numbering scheme in Figure 3.2. From the structural data given in Table 3.2, it is observed that the various bond lengths are found to be almost same at PM3 and AM1 methods. According to results of bond length and bond angle, the deformations depend on the characteristic of the substituents [12].

Table 3.2 Structural parameters calculated for chitosan employing PM3 and AM1 methods.

Bond length (Å)	PM3	AM1		Bond angle (°)	PM3	AM1
1-2	1.367	1.371				
1-3	4.589	5.531				
3-4	3.354	3.393				
4-5	1.365	1.381		1-2-6	115.268	123.573
5-6	1.485	1.362		2-6-5	98.399	96.940
6-2	3.146	3.365		6-5-4	119.376	116.572
6-7	1.257	1.361		5-4-3	150.21	148.461
7-8	0.957	0.973		4-3-1	50.956	53.858
6-9	3.681	3.909		3-1-2	100.271	103.634
1-10	1.348	1.346		2-6-7	26.025	29.504
10-11	1.099	1.086		2-6-7-8	129.148	130.086
10-12	2.182	2.189		2-6-9	13.263	18.710
10-13	1.359	1.349		2-1-10	123.171	125.225
13-14	0.951	0.968		1-10-11	126.737	121.535
1-15	3.667	3.693		10-13-14	109.542	108.531
3-16	3.192	3.148		3-17-18	108.82	108.754
3-17	1.279	1.381		4-19-20	105.369	106.559
17-18	0.958	0.971		5-22-23	116.588	113.319
4-19	1.421	1.851		5-22-24	115.174	123.844
19-20	1.019	0.961		5-6-7-8	179.005	171.428
4-21	1.914	1.233				
5-22	1.386	1.065				
5-25	0.725	1.091				
22-23	0.991	0.999				
22-24	0.992	1.001				

3.4.3 FTIR Analyses

Vibrational spectral assignments have been performed on the recorded FTIR spectra based on the theoretically predicted wave numbers using PM3 and AM1, and have been collected in table 3.3. The infrared spectrum of chitosan (Table 3.3) is typically characterized by absorption regions as follows: at 3490 cm^{-1} which is attributed to the axial stretching of O–H and CH bonds; the CH stretching bond between 5776 and 3750 cm^{-1}, NH stretching at 3541 cm^{-1}, NH asymmetric stretching at 3452 cm^{-1} indicating presence of free amino group at

C_5 of glucosamine [13], at 3427 cm^{-1} is attributed to the combined peaks of the NH$_2$ and OH group stretching vibration [14], at 1216 cm^{-1} (–NH angular deformation) and 1567 cm^{-1} (–C–O–C– in glycosidic linkage), the intensity of some bands within the range 1500–1700 cm^{-1} that are related to amino and carbonyl moieties, evidenced that these groups interact mainly through electrostatic interactions and hydrogen bonding [15-16], between 3226 and 3028 cm^{-1} (aliphatic C–H band), and at 687, 287, and 257 cm^{-1} (C–O band) [17], the band in the range 3578 and 3407 cm^{-1} attributed to O–H stretching vibrations [18] and at 1635 cm^{-1} corresponding to the chitosan NH$_2$ [19-20].

Table 3.3 *The calculated frequencies using PM3 and AM1 methods, respectively.*

ASSIGNMENT	PM3 (FREQUENCIES CM^{-1})	AM1 (FREQUENCIES CM^{-1})
CH stretching	5776	--
CH stretching	3874	--
CH stretching	3750	--
NH symmetric stretching	3541	--
NH asymmetric stretching	3452	3452
CH stretching (CH$_2$ group)	3028	--
OH stretching	2836	--
C-CH$_2$-OH	1421	1418
C=O (amide I)	1650	1645
N-H (amide II)	1555	1558
C-N (amide III)	1380	1382
C-O	1050	1051
CH, NH, CO	687	--
C-C, C-N, C-O	287	257
OH	--	3578
OH and CH stretching	--	3491
OH stretching	--	3429
OH stretching	--	3407
CH stretching	--	3226
C-C	--	2190
C-O-H	--	1567
NH$_2$	--	1216
CH	--	925
CH and OH (CH$_2$-OH)	--	518

3.4.4 Electrostatic Potential

This finding suggests that hydrogen bond interactions, either intra-chains or between polymer chains and water molecules, play for a more important role in the solubility of chitin and chitosan than hydrophobic interactions. These results have further shown that fine tuning the electrostatic contributions in chitosan can be used to promote remodeling of its the physical state. Additional simulations have shown that the overall net charge and solubility of chitosan can be altered by changes in the pH. Comparison of the electrostatic response of a chitosan and chitin chains to pH changes shows a rather distinct surface charge profile for the two polymers [11].

Figure 3.3 shows the electrostatic potential of chitosan using PM3 and AM1, respectively. A portion of a molecule that has a negative electrostatic potential is susceptible to an electrophilic attack – the more negative the better. Molecular electrostatic potential (MESP), which is related to the electronegativity and the partial charge changes on the different atoms of the chitosan molecule, when plotted on the isodensity surface of the molecule MEPS mapping is very useful in the investigation of the molecular structure with its physiochemical property relationships.
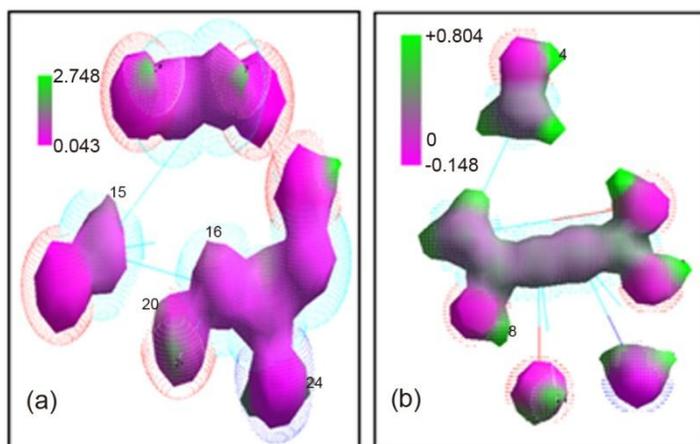
Figure 3.3 *Electrostatic potential of chitosan, in where (a) PM3 and (b) AM1, respectively.*

Pink and green areas in the MESP refer to the regions of negative and positive and correspond to the electron-rich and electron-poor regions, respectively, whereas the purple color signifies the neutral electrostatic potential [21]. The MESP in case of Figure 3.3(a) clearly suggest that each C-OH, C-H and NH bond represent the most negative potential region. Figure 3.3(b) shows

that C-C bond present neutral potential electrostatic region, C-O and NH bond represent the most negative potential region and finally the O-H represent the most negative potential region.

3.4.5 Molecular Orbitals

Hydrogen bonding, electrostatic interactions, van der Waals interactions (van der Waals bonds are mainly constructed with a balance of the exchange repulsion and dispersion attractive interactions), donor–acceptor interactions, hydrophilic–hydrophobic interactions, and $\pi-\pi$ interactions are the main types of non-covalent interactions that are responsible for self-organization in biological systems. An evidence of charge transfer (CT) complexes had been reported in solid or in solution in a different field of chemistry. The basic electronic parameters related to the orbitals in a molecule are the HOMO and LUMO (energy and symmetry) of chitosan can give us idea about the ground and excited state proton transfer processes.

The HOMO and LUMO energy calculations (see Tables 3.4-3.5) reveal the existence of interactions and according to Mulliken's theory, formation of the (CT) complex involves transition of an electron from HOMO of donor to LUMO of acceptor [8]. Its highest occupied molecular orbital (HOMO) was provided primarily by nitrogen atom and its lowest unoccupied molecular orbital (LUMO) was provided mainly by the oxygen atom. Its reaction active sites were concentrated in $-NH_2$ and $-OH$ [22]. Opposing π systems typically adopt parallelplaner (stacked or offset-stacked) geometry. The interaction between the donor and acceptor is characteristic of an electronic absorption band with low energy. One of these molecular complexes is π,π-complex between neutral molecules [8].

Table 3.4 HOMO and LUMO orbitals for chitosan using PM3 method.

ORBITAL	HOMO		LUMO	
	ENERGY (eV)	SYMMETRY (Å)	ENERGY (eV)	SYMMETRY (Å)
50	-16.60	32	-2.206	40
20	-23.25	14	1.293	55
10	-28.50	24	-1.097	45
5	-16.60	29	-2.206	40
-5	-2.215	39	-16.65	30
-10	-1.117	44	-28.19	25
-20	1.274	54	-23.71	15
-50	-2.210	39	-16.62	31

Table 3.5 *HOMO and LUMO orbitals for chitosan using AM1 method.*

ORBITAL	HOMO		LUMO	
	ENERGY (eV)	SYMMETRY (Å)	ENERGY (eV)	SYMMETRY (Å)
50	-12.57	31	2.492	42
20	-18.31	16	6.102	57
10	-14.22	26	4.502	47
5	-12.57	31	2.495	42
-5	2.489	41	-12.56	32
-10	4.058	46	-14.23	27
-20	6.092	56	-18.36	17
-50	2.489	41	-12.46	32

3.4.6 Conclusions

Empirical and semi-empirical mathematical models can be used to describe experimentally models are mechanistic theories. Molecular modeling is particularly useful to understand interactions between various kinds of molecules with different methods. The geometries energies of chitosan were computed by means of AM1 and PM3 methods. These calculations allowed us to retrieve the minimal energy conformation and investigate all possible conformations. The calculations confirmed that the most stable interactions involved the free amino site in a "pending complex". FTIR results are very similar between the different methods of analysis. The main absorption peaks of chitosan are observed at 1650-1645 cm^{-1}, attributed to C=O stretching (amide I), at 1558-1555 cm^{-1}, assigned to N-H bending (amide II), and at 1382-1380 cm^{-1}, assigned C-N stretching (amide III). The absorption peak at 1050 cm^{-1} is assigned to C-O stretching and the broad band above 3000 cm^{-1} corresponds to O-H and N-H bonds. Simultaneous structural parameters and IR of the different methods provide evidence for the charge transfer interaction between the donor and the acceptor groups. Vibrational analysis confirms that intramolecular charge transfer (ICT) must be responsible for the optical nonlinearity of the molecule. HOMO and LUMO energy gap explains the eventual charge transfer interactions taking place within the molecule. MESP plays an important role in determining stability of the molecule.

References

[1] Aranaz I, Meng bar M, Harris R, Pa ños I, Miralles B, Acosta N, Galed G and Heras A, Functional Characterization of Chitin and Chitosan, *Current Chemical Biology*, 3, 203-230, 2009.

[2] Park C J, Gabrielson N P, Pack D W, Jamison R D, Johnson A J W. The effect of chitosan on the migration of neutrophil-like HL60 cells, mediated by IL-8, *Biomaterials.* 30, 436–444, 2009.

[3] Zhuangdong Y. Study on the synthesis and catalyst oxidation properties of chitosan bound nickel (II) complexes. *Chemical Industry Times*. 21(5), 22–24, 2007.

[4] Kean T, Roth S, Thanou M. Trimethylated chitosans as non-viral gene delivery vectors: cytotoxicity and transfection efficiency. *J Control Release.* 103(3), 643–53, 2005.

[5] Alves N M, Mano J F, Chitosan derivatives obtained by chemical modifications for biomedical and environmental applications, *International Journal of Biological Macromolecules.* 43, 401–414, 2008.

[6] Mertins O, Dimova R. Binding of Chitosan to Phospholipid Vesicles Studied with Isothermal Titration Calorimetry, *Langmuir.* 27, 5506–5515, 2011.

[7] Hemalatha R, Chitra R, Rathinam J R, Sudha. P N, Synthesizing and characterization of chitosan graft co polymer: adsorption studies for Cu (II) and Cr (VI), *International Journal Of Environmental Sciences*. 2(2), 805-828, 2011.

[8] Shihab M S, AM1 semi-empirical calculation to study the nature of di- and tri-molecular assembly of π,π-aromatic interactions, *The Arabian Journal for Science and Engineering.* 35(2A), 95-113, 2010.

[9] Kumar P, Choonara Y E, Du Toit L C, Modi G, Naidoo D and Pillay V. Novel High-Viscosity Polyacrylamidated Chitosan for Neural Tissue Engineering: Fabrication of Anisotropic Neurodurable Scaffold via Molecular Disposition of Persulfate-Mediated Polymer Slicing and Complexation, *Int. J. Mol. Sci.* 13, 13966-13984, 2012.

[10] Zhu H Y, Fu Y Q, Jiang R, Yao J, Xiao L, Zeng G M, Novel magnetic chitosan/poly(vinyl alcohol) hydrogel beads: preparation, characterization and application for adsorption of dye from aqueous solution, *Bioresour Technol.* 105, 24-30, 2012.

[11] Cunha R A, Franca E F, Soares T A, Rusu V H, Pontes F J S and Lins R D. The Molecular Structure and Conformational Dynamics of Chitosan Polymers: An Integrated Perspective from Experiments and Computational Simulations, Biochemistry, Genetics and Molecular Biology. The Complex World of Polysaccharides. book edited by Desiree Nedra Karunaratne, ISBN 978-953-51-0819-1, Chapter 9.

[12] Kalninsh K K. Joint Experimental And Theorical study of the poly (styryl sodium) and poly (a-methylstyryl sodium) polymerization*/* depolymerization. *Phys. Chem. Chem. Phys.* 3, 4542-4546, 2001.

[13] Jindal M, Kumar V, Rana V, Tiwary A K, Physico-chemical, mechanical and electrical performance of bael fruit gum–chitosan IPN films, *Food Hydrocolloids*, 30(1), 192-199, 2013.

[14] AbdElhady M M. Preparation and Characterization of Chitosan/Zinc Oxide Nanoparticles for Imparting Antimicrobial and UV Protection to Cotton Fabric, *International Journal of Carbohydrate Chemistry*, 1-6, 2012.

[15] Yuan Y, Wan Z L, Yin S W, Yang X Q, Qi J R, Liu G Q, Zhang Y, Characterization of complexes of soy protein and chitosan heated at low pH. *Food Science and Technology*, 50(2), 657-664, 2013.

[16] Pereira A E. Aldehyde-functionalized chitosan and cellulose:chitosan composites: application as drug carriers and vascular bypass grafts, Thesis for the Doctor of Philosophy degree in Pharmacy (Pharmaceutics), University of Iowa, 2011.

[17] Lertsutthiwong P, Noomun K, Khunthon S, Limpanart S. Influence of chitosan characteristics on the properties of biopolymeric chitosan–montmorillonite.

[18] George T S, Guru K S, Sankaranarayanan V N, Packiam K K. Extraction, Purification And Characterization Of Chitosan From Endophytic Fungi Isolated From Medicinal Plants. *World Journal of Science and Technology*, 1(4), 43-48, 2011.

[19] Islam M, Masum S, Rahman M, Molla A I, Shaikh A A, Roy S K. Preparation of Chitosan from Shrimp Shell and Investigation of Its Properties, *International Journal of Basic & Applied Sciences IJBAS-IJENS.* 11(01), 116-130, 2011.

[20] Britto D, Assis B G. Synthesis and mechanical properties of quaternary salts of chitosan-based films for food application. *International Journal of Biological Macromolecules*. 41(2), 198-203, 2007.

[21] Gayathri R, Arivazhagan M. Experimental (FTIR an FT-Raman) and theretical

(HF and DFT) investigation, NMR, NBO, electronic properties and frequency estimation analyses on 2,4,5.trichlorobenzene sulfonyl cl¿hloride. *Spectrochiica Acta Part A: Molecular and Biomolecular Spectroscopy*. 97, 311-325, 2012.

[22] Balanta D, Grande C D, Zuluaga F. Extracci ón, Identificaci ón y Caracterizaci ón de Quitosano del Micelio de *Aspergillus Niger y* Sus Aplicaciones Como Material Bioadsorbente en el Tratamiento de Aguas, *Revista Iberoamericana de Pol íneros.* 11(5), 297-316, 2010.

Chapter 4

Polyvinylpyrrolidone (PVP)

Chapter 4

Polyvinylpyrrolidone (PVP)

NORMA AUREA RANGEL-VÁZQUEZ[1]
FRANCISCO RODRÍGUEZ FÉLIX[2]
BÁRBARA-SUSANA GREGORÍ VALDÉS[3]

[1]*División de Estudios de Posgrado e Investigación del Instituto Tecnológico de Aguascalientes, Ave. López Mateos # 1801 Ote. Fracc. Bona Gens CP. 20256 Aguascalientes, Aguascalientes, México*

[2]*Departamento de Investigación y Posgrado en Alimentos. Universidad de Sonora, Blvd. Luis Encinas y Rosales S/N Col. Centro, Hermosillo, Sonora, México*

[3]*Institute for Biotechnology and Bioengineering, Centre for Biological and Chemical Engineering, Instituto Superior Técnico, Av. Rovisco Pais 1, 1049-001 Lisboa, Portugal*

Abstract

In this study, molecular simulations of polyvinylpyrrolidone (PVP) were obtained using PM3 and AM1 methods containing. PVP was characterized by FTIR, electrostatic potential, molecular orbitals, respectively. The results of the computer simulation indicated that a Gibbs free energy is very similar between two methods.

Keywords: PVP, Simulation, PM3, AM1

4.1 Introduction

The chemistry of acetylene, developed at BASF in the 1920s byWalter Reppe, opened up numerous application possibilities, especially in the young field of plastics. In 1938, the year Nylon and Perlon were discovered, BASF succeeded in using acetylene chemistry to develop a highly interesting derivative: by reacting acetylene with pyrrolidone, vinylpyrrolidone was obtained, which in turn was used to form polyvinylpyrrolidone (PVP). The process patent was granted on January 1, 1939. It soon became apparent that PVP was an all-

around talent. It is readily soluble in water, physiologically compatible, non-toxic, essentially chemically inert, temperature-resistant, pH-stable, non-ionic, and colorless. This remarkable combination of properties predestined its use in numerous applications in medicine, pharmaceutical technology, cosmetics, and in the technical industry. Even as early as 1939, PVP was used as a plasma expander and was widely used in this form during World War II. During the 1950s, PVP replaced the schellac hitherto used in hair sprays [1].

4.2 Synthesis and Structure

PVP is soluble in water and other polar solvents. When dry it is a light flaky powder, which readily absorbs up to 40% of its weight in atmospheric water. In solution, it has excellent wetting properties and readily forms films. This makes it good as a coating or an additive to coatings. PVP is a branched polymer, meaning its structure is more complicated than linear polymer, though it too lies in a two-dimensional plane. In general, compositions of polymers are made up of many simple molecules that are repeating structural units called monomers.

A single polymer molecule may consist of hundreds to a million monomers and may have a linear, branched, or network structure. Covalent bonds hold the atoms in the polymer molecules together and secondary bonds then hold groups of polymer chains together to form the polymeric material. Copolymers are polymers composed of two or more different types of monomers [2]. PVP is synthesized via a free radical polymerization reaction starting from the vinylpyrrolidone (VP) monomer, using a free radical initiator such as Azobisisobutyronitrile (AIBN) (see Figure 4.1) [3].
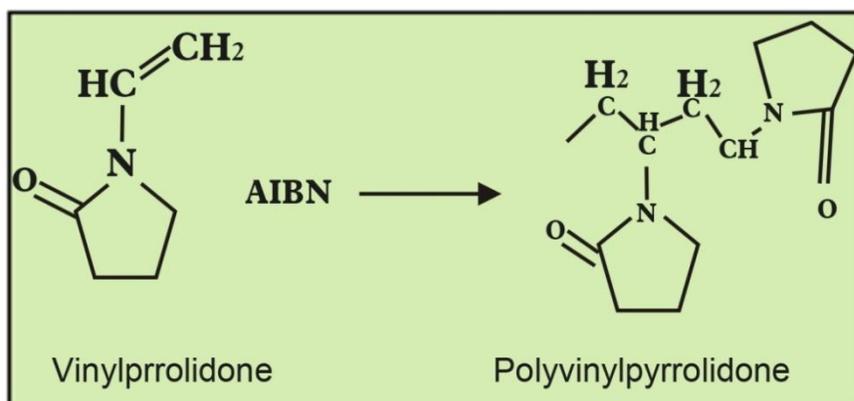
Figure 4.1 *Reaction for the synthesis of polyvinylpyrrolidone.*

4.3 Applications

The polymer PVP was used as a blood plasma expander for trauma victims after the 1950s. It is used as a binder in many pharmaceutical tablets; it simply passes through the body when taken orally. However, autopsies have found that crospovidone does contribute to pulmonary vascular injury in substance abusers who have injected pharmaceutical tablets intended for oral consumption. The long-term effects of crospovidone within the lung are unknown. PVP added to iodine forms a complex called povidone-iodine that possesses disinfectant properties. This complex is used in various products like solutions, ointment, pessaries, liquid soaps and surgical scrubs. It is known under the trade name Betadine and Pyodine. It is used in pleurodesis (fusion of the pleura because of incessant pleural effusions). For this purpose, povidone iodine is equally effective and safe as talc, and may be preferred because of easy availability and low cost [4-6].

4.4 Results and Discussion of Simulations Analyses

4.4.1 Optimization Energy

Table 4.1 shows the Gibbs energy free for PVP structure using different methods, in where the negative values of ΔG by means different methods shows that the electrostatic binding is energetically favorable. The difference in the energy values are attributed to the formula of the method applied [7]. Attractive interaction between π systems is the interaction between two or more molecules leading to self-organization by formation of a complex structure which has lower conformation equilibrium than of the separate components and shows different geometrical arrangement with the AM1 and PM3 method (Figure 4.2).

Table 4.1 *Gibbs energy free for PVP structure.*

Method	ΔG (Kcal/mol)
AM1	-1494
PM3	-1626
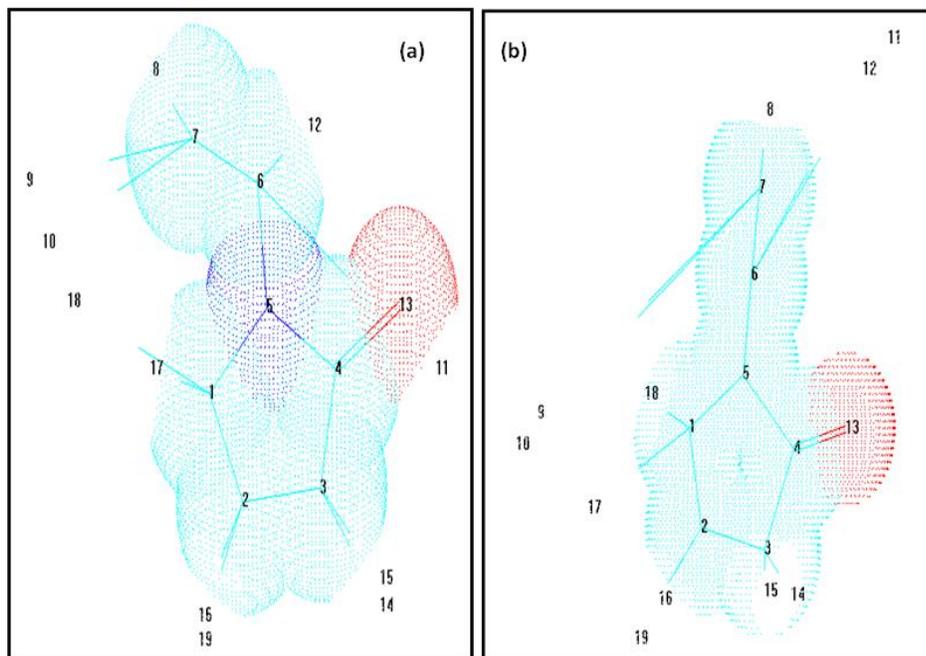
Figure 4.2 *Molecular geometry of PVP, in where (a) PM3 and (b) AM1, respectively.*

4.4.2 Structural Parameters

From the structural data given in Table 4.2, it is observed that the various bond lengths and angles are found to be very same at PM3 and AM1 methods. For the title molecule, the PVP is planar, and also CH_3-CH_2 (6-11 atoms) attached to nitrogen element (atom #5) as evident from the bond lengths and angles. According to their observations, deformations of the PVP structure depend of CH bond of the PVP ring [8].

Table 4.2 *Structural parameters calculated for PVP employing PM3 and AM1 methods.*

Bond length (Å)	PM3	AM1
1-2	1.37	1.37
2-3	1.41	1.41
3-4	1.38	1.38
4-5	1.42	1.42
5-1	1.42	1.42
5-6	1.42	1.42
6-7	1.32	1.32
6-11	3.85	3.81
6-12	1.10	1.01
7-8	1.06	1.06
7-9	3.05	3.03
7-10	2.99	2.97
4-13	1.36	1.36
3-14	1.65	1.65
3-15	1.65	1.65
2-16	1.66	1.66
2-19	1.68	1.67
1-17	1.09	1.10
1-18	2.76	2.76

Bond angle (°)	PM3	AM1
1-2-3	109.8	109.7
2-3-4	107.75	107.8
3-4-5	107.74	107.7
4-5-1	107.77	107.8
5-1-2	106.9	106.8
1-17-18	6.970	7.52
2-16-19	25.29	25.32
3-14-15	25.58	25.57
3-4-13	133.0	133
4-5-13	119.24	119.23
5-6-11	51.04	51.6
6-11-12	65.3	66
6-7-8	157.24	156.91
6-7-10	130.39	130
7-8-9	57.26	57.6
7-9-10	15.09	15.19

4.4.3 FTIR Analyses

The resulting vibrational frequencies for the optimized geometries and the proposed vibrational assignments as well as FTIR also given in Table 4.3 in where, the results are very similar between AM1 and PM3 method. From 4328 to 4279 corresponds to CH_2 symmetric stretching, from 3329 at 2976 cm^{-1} were attributed at CH stretching, at 2263 was assigned to CH (CH_3-CH_2), at 1420-1500 cm^{-1} of the CH_3 scissoring, at 1651 cm^{-1} the C–N stretching reveal the characteristic absorbance peak of PVP [9-12]. The peak between 2194 at 2121cm^{-1} is assigned to the stretching vibration of the C=O in the PVP amide unit [12-13]. The C=O groups of pure PVP show a prominent peak at 1663 cm^{-1} in FTIR spectrum. This characteristic peak can be investigated to explore about the interaction between PVP and metal species [14-15].

Table 4.3 *The calculated frequencies using PM3 and AM1 methods, respectively.*

ASSIGNMENT	PM3 (FREQUENCIES CM^{-1})	AM1 (FREQUENCIES CM^{-1})
CH (CH$_2$) symmetric stretching	---	4328
CH (CH$_2$) symmetric stretching	---	4279
CH stretching	---	3329
CH stretching	3179	3182
CH stretching	3058	3061
CH stretching	2976	2976
CH (CH$_2$) symmetric stretching	---	2839
CH (CH$_3$-CH$_2$) stretching	---	2263
C=O stretching	2194	2121
C-N	---	1651
CH deformation of cycli CH$_2$ groups	1489	1492
C-C (PVP ring)	1386	1382
C-C (PVP ring)	---	1321
Amide or CH$_2$ rock	730	733
CH deformations	618	618
C-N, C-C	658	---

4.4.4 Electrostatic Potential

Figure 4.3 shows the electrostatic potential of the PVP using PM3 and AM1 method, where Figure 4.3(a) shows that the CH$_3$-CH$_2$ bond presents a neutral electrostatic potential, while in the area of green color of CH bond of the PVP ring is attributed to positive values of the potencal, in fact, reppresenta electron-poor regions, while ring like C-N bond presented the negative regions, i.e., where the majority of electrons are, while Figure 4.3(b) shows that, C-C and C-N ring bonds shown positive potentials and the CH$_3$-CH$_2$ bond characteristic potential is negative, these differences are due to the method used to determine the values maximum and minimum of the electrostatic potential of the PVP.

4.4.5 Molecular Orbitals

The excitation band is attributed to the electronic transitions in PVP molecular orbitals. Alternatively, the blue emission band of PVP at 394 nm is attributed to the radiative relaxation of electrons from the lowest energy unoccupied molecular orbital (LUMO) to the highest energy occupied

molecular orbital (HOMO) levels in PVP [16].
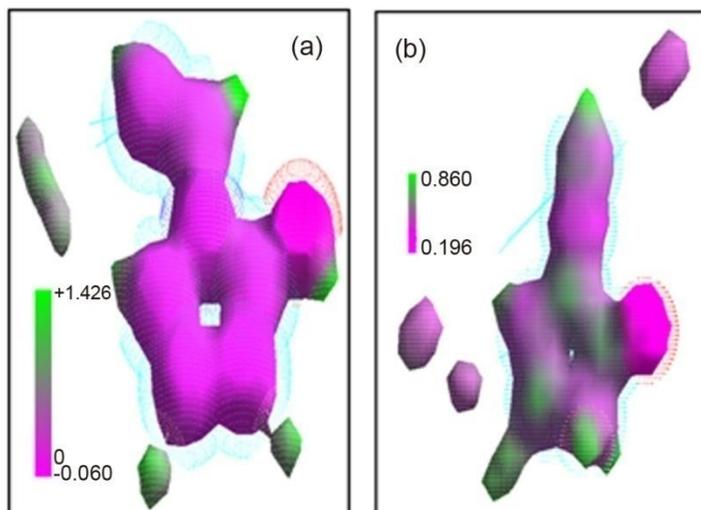
Figure 4.3 *Electrostatic potential of PVP, in where (a) PM3 and (b) AM1, respectively.*

Table 4.4 *HOMO and LUMO orbitals for PVP using PM3 method.*

ORBITAL	HOMO		LUMO	
	ENERGY (eV)	**SYMMETRY (Å)**	**ENERGY (eV)**	**SYMMETRY (Å)**
50	-14.25	16	1.86	27
20	-39.51	1	6.62	42
10	-16.38	11	4.03	32
5	-14.25	16	1.86	27
-5	1.731	26	-13.20	17
-10	3.563	31	-15.88	12
-20	6.134	41	-36.68	2
-50	1.730	26	-13.20	17

Table 4.5 *HOMO and LUMO orbitals for PVP using AM1 method.*

ORBITAL	HOMO		LUMO	
	ENERGY (eV)	SYMMETRY (Å)	ENERGY (eV)	SYMMETRY (Å)
50	-18.08	16	-2.59	27
20	-45.76	1	1.76	42
10	-20.51	11	-1.40	32
5	-18.08	16	-2.59	27
-5	-3.59	26	-17.94	17
-10	-1.56	31	-20.13	12
-20	1.37	41	-42.58	2
-50	-3.59	26	-17.94	17

4.4.6 Conclusions

As a consequence of the development of theory, computers and computer software, molecular orbital model calculations are important tools in all branches of chemistry. The quantum mechanical models help us to explain, and to better understand, the physical cause of isotope substitution effect using different techniques of analysis. In this work, the PVP was analyzed using PM3 and AM1 method, in where both results confirm all the typical adsorption bands of PVP. These methods can be used quite satisfactorily in predicting the chemical reactivity of the molecules and the effect of substitution of either donor electron or acceptor electron.

References

[1] Folttmann H, Quadir A. Polyvinylpyrrolidone (PVP) – One of the Most Widely Used Excipients in Pharmaceuticals: An Overview. *Drug Delivery Technology.* 8(6), 22-27, 2008.

[2] Fischer Frank; Bauer Stephan. Polyvinylpyrrolidon. Ein Tausendsassa in der Chemie. *Chemie in unserer Zeit.* 43(6), 376–383, 2009.

[3] http://web.njit.edu/~mitra/green_chemistry/EXP_2.htm.

[4] Bühler V. *Excipients for Pharmaceuticals - Povidone, Crospovidone and Copovidone*. Berlin, Heidelberg, New York: Springer. pp. 1–254.

[5] Ganesan S. Embolized Crospovidone (poly[N-vinyl-2-pyrrolidone]) in the Lungs of Intravenous Drug Users. *Modern Pathology.* 16(4), 286–292, 2003.

[6] Das S K, Saha S K, Das A, Halder A K, Banerjee S N, Chakraborty M. A study of comparison of efficacy and safety of talc and povidone iodine for pleurodesis of malignant pleural effusions. *Journal of the Indian Medical Association.* 106(9), 589–592, 2008.

[7] Laot C M. Spectroscopic Characterization of Molecular Interdiffusion At A Poly(Vinyl Pyrrolidone)/ Vinyl Ester Interface. Thesis of Master of Science in Chemical Engineering. Virginia Polytechnic Institute and State University. 1997.

[8] Gayathri R, Arivazhagan M. Experimental (FTIR an FT-Raman) and theretical (HF and DFT) investigation, NMR, NBO, electronic properties and frequency estimation analyses on 2,4,5.trichlorobenzene sulfonyl cl¿hloride. *Spectrochiica Acta Part A: Molecular and Biomolecular Spectroscopy*. 97, 311-325, 2012.

[9] Britto D, De-Assis O. Synthesis and mechanical properties of quaternary salts of chitosan-based films for food application. *International Journal of Biological Macromolecules.* 41(2), 198-203, 2007.

[10] Kaèmierska K A, Kuc K, Ciach T. Polyvinylpyrrolidone-Polyurethane Interpolymer Hydrogel Coating As A Local Drug Delivery System. *Acta Poloniae Pharmaceutica ñ Drug Research*. 65(6), 763-766, 2008.

[11] Koo C M, Ham H T, Choi M H, Kim S O, Chung I J. Characteristics of polyvinylpyrrolidone-layered silicate nanocomposites prepared by attrition ball milling. *Polymer*. 44, 681–689, 2003.

[12] Li Z, Zhang J, Mu T, Du J, Liu Z, Han B, Chen J. Preparation of polyvinylpyrrolidone-protected Prussian blue nanocomposites in microemulsion. *Colloids and Surfaces A: Physicochem. Eng. Aspects.* 243, 63–66, 2004.

[13] Fung-Tan Y, Khiang K, Al-Hanbali O. Investigation of interpolymer complexation between Carbopol and various grades of polyvinylpyrrolidone and effects on adhesion strength and swelling properties. *J Pharm Pharmaceut Sci.* 4(1), 7-14, 2001.

[14] Tu W X. Study on the Interaction Between Polyvinylpyrrolidone And Platinum Metals During The Formation Of The Colloidal Metal Nanoparticles. *Chinese Journal Of Polymer Science.* 26(1), 23−29, 2008.

[15] Wang W, Wang Q, Wang A. pH-Responsive Carboxymethylcellulose-*g*-Poly

(sodium acrylate)/Polyvinylpyrrolidone Semi-IPN Hydrogels with Enhanced Responsive and Swelling Properties. *Macromolecular Research*. 19(1), 57-65, 2011.

[16] Thi T M, Tinh L V, Van B H, Ben P V, Trung V Q. The Effect of Polyvinylpyrrolidone on the Optical Properties of the Ni-Doped ZnS Nanocrystalline Thin Films Synthesized by Chemical Method. *Journal of Nanomaterials*. 2012, 1-8, 2012.

Chapter 5

Mimosa Tenuiflora

Chapter 5

Mimosa Tenuiflora

NORMA AUREA RANGEL-VÁZQUEZ[1]
FRANCISCO RODRÍGUEZ FÉLIX[2]

[1]*División de Estudios de Posgrado e Investigación del Instituto Tecnológico de Aguascalientes, Ave. López Mateos # 1801 Ote. Fracc. Bona Gens CP. 20256 Aguascalientes, Aguascalientes, México*
[2]*Departamento de Investigación y Posgrado en Alimentos. Universidad de Sonora, Blvd. Luis Encinas y Rosales S/N Col. Centro, Hermosillo, Sonora, México*

Abstract

The bark of Mimosa tenuiflora is a traditional remedy for several skin ailments like burns, ulcer and psoriasis and plays furthermore a role in the treatment of wounds. For ethnopharmaceutical use the bark is usually powdered and often applied as decoct or cataplasm. According to the studies performed with Mimosa tenuiflora to the present, it seems that the wound-healing activity of this plant is due to a combination of the several different compounds (tannins and flavonoid mainly). In this chapter, the structure of the tannin and flavonoid was analyzed by PM3 and AM1 methods since represent the main constituents of the Mimosa tenuiflora. It is determined by the electrostatic potential and the molecular orbitals that the hydroxyl group of the flavonoid structure it is attracted by the oxygen present in the carbonyl group of the structure of tannins. In addition to the main signals of FTIR analyses.

Keywords: Mimosa Tenuiflora, PM3, AM1

5.1 Introduction

Mimosa hostilis is the former scientific name for *Mimosa tenuiflora*, and the two names are synonymous [1-2]. The older name is still widely know due to its presence in the literature and as distributers of botanical products still use the older term. *M. tenuiflora* is an entheogen known as *Jurema*, *Jurema Preta*,

Black Jurema, and *Vinho de Jurema*. Dried Mexican *Mimosa Hostilis* root bark has been recently shown to have a DMT content of about 1%. The stem bark has about 0.03% DMT (Figure 5.1).

Figure 5.1 Mimosa tenuiflora.

To date no β-carbolines such as harmala alkaloids have been detected in *Mimosa tenuiflora* decoctions, however the isolation of a new compound called "Yuremamine" from *Mimosa tenuiflora* as reported in 2005 represents a new class of phyto-indoles [3]. This may explain the reported oral activity of DMT in Jurema without the addition of an MAOI. Imported MHRB typically requires the addition of an MAOI in the preparation of ayahuasca.

In Mexico in 1984, this natural resource was utilized empirically to alleviate the sufferings of hundreds of victims of large natural-gas depot explosion; on that occasion, direct application of powdered *Mimosa tenuiflora* bark on patients' burns resulted in facilitation of skin regeneration and prevention of scarring in many of the patients. Subsequently, news of the existence of a miraculous Mexican tree skin was spread worldwide by the mass media, producing a rise in spotlighting commercial attention on this natural product and included the elaboration of several products with supposed medicinal properties.

During the 1990s pharmacological and phytochemical studies performed by Mexican research groups supported the existence of natural compounds with cicatrizing properties in *Mimosa tenuiflora* cortex. A series of pre-clinical experimental studies concluded that water and alcoholic extracts obtained from the dried bark of *Mimosa tenuiflora* are particularly rich in tannins and that these also contain steroidal saponins biological activity of these extracts was defined as (a) possessing strong *in vitro* antimicrobial properties against a wide

group of microorganisms, yeasts, and dermatophytes and (b) inducing the growth *in vitro* of fibroblasts and other human cells [4].

5.2 Secondary Metabolites of *Mimosa Tenuiflora*

The phytochemistry of *M. tenuiflora* has attracted considerable interest, mainly due to the presence of indole alkaloids and tannins (proanthocyanidins). However, phytochemical reports on others classes of the compounds that may be present are rare.

- **Alkaloids**

Two indole alkaloids have been isolated from "jurema": 5-hydroxy-tryptamine, and N, N-dimetyltryptamine. The latter is also found in the root bark, and is linked to its hallucinogen use, as mentioned above. The alkaloid N, N-dimetyltryptamine was apparently detected for the first time by Gonçalves de Lima and his team, after a visit to the Pancararu village in Brejo dos Padres (Pernambuco state, northeastern Brazil). The substance isolated was called nigerine. Ott (2002), however, suggested that this product could be an impure form of N, N-dimetyltryptamine. Vepsäläinen et al. (2005) performed one phytochemical study of this species with advanced instrumentation and methodologies, particularly [1]H-^{13}C nuclear magnetic resonance (NMR) and liquid chromatography-mass spectrometry (LC-MS) under mild acidic pH. A new phytoindole, Yuremamine, was isolated from the stem bark of *M. tenuiflora* in this study (Figure 5.2).
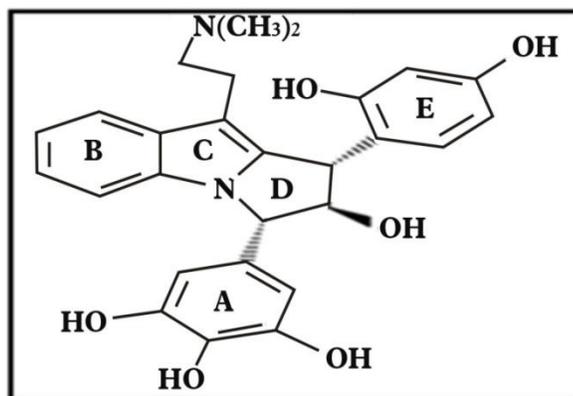
Figure 5.2 *Yuremamine from the stem bark of Mimosa tenuiflora.*

- **Chalcones**

Other studies demonstrated the presence of two chalcones: kukulkan A (2',4'-dihydroxy-3',4-dimetoxychalcone); and kukulkan B (2',4',4-trihydroxy-3'-metoxychalcone)((Figure 5.3).
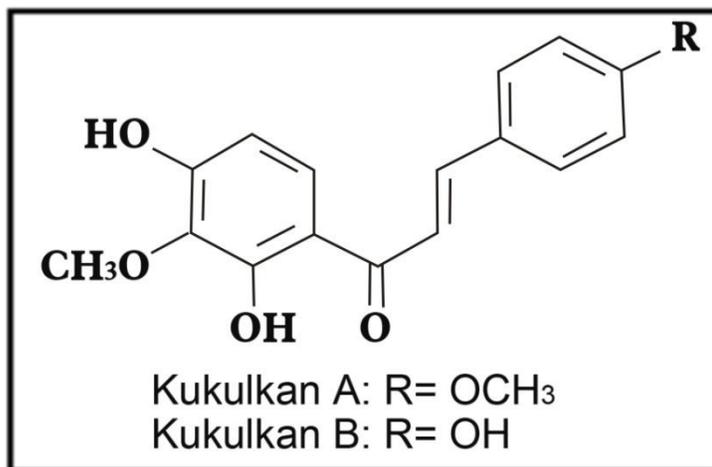
Figure 5.3 *Chalcones isolated from the stem bark of Mimosa tenuiflora.*

- **Steroids and Terpenoids**

Among the several substances three steroids were isolated from the stem bark of *M. tenuiflora*: campesterol-3-O-beta-D-glucopyranosyl, stigmasterol-3-O-beta-D-glucopyranosyl, and beta-sitosterol-3-O-beta-D-glucopyranosyl. Three saponins have also been identified: mimonoside A, mimonoside B, and mimonoside C (Figure 5.4). Anton et al recorded the presence of the triterpenoid lupeol.
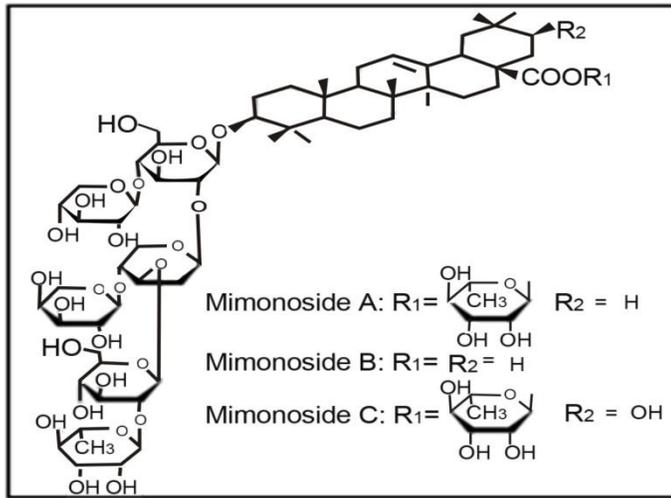
Figure 5.4 *Triterpenoids saponins isolated from the stem bark of Mimosa tenuiflora.*

- **Phenoxychromones**

Five 2-phenoxychromones ("uncommon" flavonoids), the tenuiflorin A [5, 7-dihydroxy-2-(3-hydroxy-4-methoxyphenoxy)-6 methoxychromone], tenuiflorin B [5, 7-dihydroxy-2- (4-hydroxy-3-methoxyphenoxy)-6-methoxychromone] and tenuiflorin C [5,7-dihydroxy-2-(3-hydroxy-4-methoxyphenoxy)-chromone], along with 6-demethoxycapillarisin and 6-demethoxy-4'-O-methylcapillarisin were isolated from the leaves of *M. tenuiflora* (Figure 5.5). These uncommon "flavonoids" exhibited an unusual ether linkage between the B and C ring.
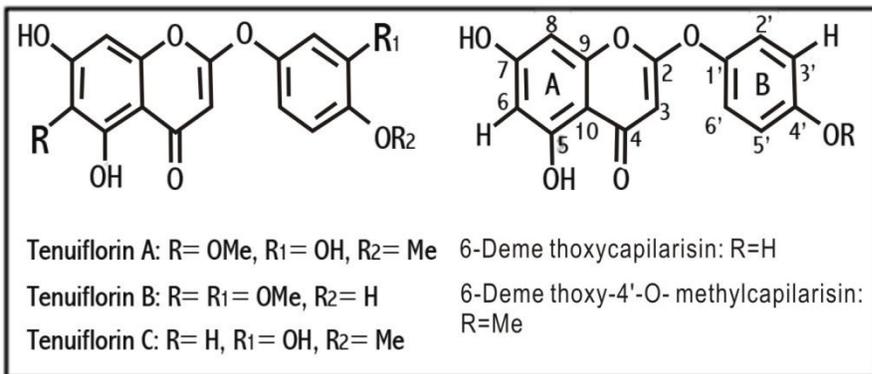
Figure 5.5 *Phenoxychromones isolated from the leaves of Mimosa tenuiflora.*

- Pharmacological Studies of the Extracts

1) Antimicrobial activity

Tables 5.1 and 5.2 show results of the experiments undertaken to test for any antimicrobial activity of the substances from the bark of *M. tenuiflora*. Tannins are probably responsible for most of this activity. An ethanol extract (95 %) was active against *Micrococcus luteus* and *Bacillus subtilis.* Table 5.2 lists the species of the fungi (*Microsporum canis*, *Microsporum gypseum*, *Trichophyton mentagrophytes*, *Trichophyton rubrum*, and *Chaetomium indicum*) against which the activity was observed. The substances extracted with ethanol (95%) were also effective against *Candida albicans*.

Table 5.1 *Antibacterial activity related from Mimosa tenuiflora.*

EXTRACT /ACTIVE DOSE	RESULTS /TESTED MICROORGANISM
Buthanol 5 mg/well	*Staphylococcus aureus*
Buthanol 15 mg/well	*Escherichia coli*
Methanol 5 μg/well	*Staphylococcus aureus*
Methanol 15 μg/well	*Escherichia coli*
Ethyl Acetate 5 mg/well	*Escherichia coli*
Ethyl Acetate 10 mg/well	*Staphylococcus aureus*
Ethanol (95%) MIC > 10 μg/mL	*Staphylococcus epidermidis and Acinetobacter calcoaceticus*
Ethanol (95%) MIC 10 μg/mL	*Staphylococcus aureus Micrococcus luteus*
Ethanol (95%) MIC 20 μg/mL	*Escherichia coli and Klebsiella pneumoniae*
Ethanol (95%) MIC 40 μg/mL	*Pseudomonas aeruginosa*
Ethanol (95%) 5 μg/disc	*Escherichia coli*
Ethanol (95%) 5 μg/disc	*Bacillus subtilis*
Ethanol (95%) 5 μg/disc	*Micrococcus luteus*

Table 5.2 *Antifungical activity related from Mimosa tenuiflora.*

EXTRACT / ACTIVE DOSE	RESULTS / TESTED MICROORGANISM
Ethanol (95%) MIC 10 μg/mL	*Microsporum canis, Microsporum gypseum, Trichophyton mentagrophytes, Trichophyton rubrum and Chaetomium indicum*
Ethanol (95%) 10 μg/mL	*Penicillium oxalicum*
Ethyl acetate 30 mg/well	*Candida albicans*
Ethanol (95%) MIC 70 μg/mL	*Candida albicans*

2) Antiinflammatory and healing action

Tellez and Dupoy de Guitard demonstrated the effectiveness of *Mimosa tenuiflora* in the topical treatment of the eczema (10% concentration), as well as against the inflammations (as a powder made from the dry bark) in the humans. In a similar experiment, the use of the dry bark of *Mimosa tenuiflora* proved to be effective in wound healing and in the treatment of venous leg ulceration disease.

3) Antispasmolytic action

Meckes-Lozoya et al., using a spray of the bark extract, observed (Table 5.3), the inhibition of the intestinal peristalsis due to a relaxation of the ileum smooth muscle tissue; an increase in the muscular tonus and in the frequency of the contractions of the uterus segments; and an increase in the muscular tonus of the stomach walls. All these experiments were performed with the rats and guinea pigs.

The butanol extract was the most efficient, and contained the most alkaloids. A fraction containing the indolalkylamine and three other smaller bases were responsible for inhibiting the peristaltic reflex of the intestine, resulting in the relaxation of the ileum observed in the guinea pigs.

4) Hemolytic activity

Mekces-Lozoya et al. reported the hemolytic activity of the raw extracts of the stem bark (Table 5.3). Triterpenic saponines, the substances considered responsible for this activity, cause membrane rupture in the erythrocytes. Studies undertaken in 1992 detected a hemolytic effect in low concentrations of a methanol extract containing alkaloids, and a haemagglutinant effect in high doses [5].

Table 5.3 *Biological activities from crude extracts of Mimosa tenuiflora (wild) poir.*

ACTIVITY	TESTED IN	EXTRACT / CONCENTRATION	RESULT
Hemolytic	Erythrocytes	Buthanol 250 µg/mL	74% of hemolyse
		Ethyl acetate 250 µg/mL	48% of hemolyse
		Methanol 500 µg/mL	68% of hemolyse
Wound healing	Adult human external use	10%	Active
		Not related (powder)	Active
Alteration in muscular tonus	Guinea pig and mouse (all the tests)	Buthanol 30 µg/mL	Increase of muscular tonus and the frequency of contraction of the uterus. Active in stomach (increase muscular tonus in rats and relaxation in guinea pig) and ileum (relaxation)
		Ethyl acetate 30 µg/mL	
		Methanol 30 µg/mL Alkaloid crude fraction 100 µg/mL	
	Guinea pig	Alkaloid crude fraction 25 µg /mL and 35 µg/mL	Inhibition of the peristaltic reflex (ileum)

5.3 Results and Discussions of Simulations Analyses

5.3.1 Optimization Energy

Table 5.4 shows the Gibbs energy free of *Mimosa tenuiflora* using PM3 and AM1 methods. In this table can be observed that the negatives values of *Mimosa tenuiflora* are energetically favorable. Figure 5.6 shows that the hydroxyl group (17-27 bond) of the flavonoid structure it is attracted by the oxygen present in the C=O bond (carbonyl group) of the structure of tannin (7-10 bond), because of attractions by hydrogen bonds. Is important mention that

with both methods the obtained geometry (ΔG) is appropriate to carry out a reaction, however applying the PM3 method gets a major attraction due to the equation of this method.

These interactions play important roles in the chemical reaction. So, the *Mimosa tenuiflora* bark got into strong focus of modern scientific investigation of skin treatment [6].

Table 5.4 *Gibbs energy free for Mimosa tenuiflora structure.*

Method	ΔG (Kcal/mol)
AM1	- 6005
PM3	- 6372
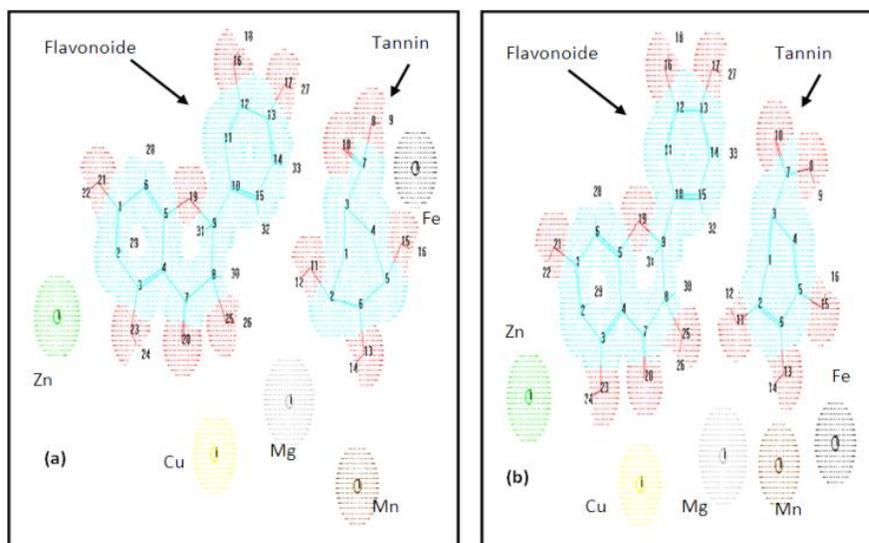
Figure 5.6 *Geometry optimization (ΔG) of Mimosa tenuiflora, where (a) PM3 and (b) AM1 method.*

5.3.2 Structural Parameters

The results of structural parameters of the structure of the tannin and flavonoid main constituents of *Mimosa tenuiflora*, through the application of PM3 and AM1 semi-empiric methods, are shown in Tables 5.5 and 5.6 respectively. These results in conjunction with Figure 5.6 indicate that both structures are not linear. It fact, the large quantity of hydroxyl groups (Figure 5.6) of the flavonoids makes them highly reactive, providing numerous focal

points capable of forming hydrogen bonds being the reason why form reversible associations with the flavonoids of *Mimosa tenuiflora* [7].

Table 5.5 *Structural parameters of flavonoids structure.*

Bond length (Å)	PM3	AM1	Angle (Å)	PM3	AM1
1-2	1.36	1.33	1-2-3	124.12	122.34
2-3	1.52	1.48	2-3-4	120.22	118.98
3-4	1.41	1.34	3-4-5	115.34	113.72
4-5	1.60	1.55	4-5-6	123.97	122.90
5-6	1.37	1.31	5-6-1	117.46	116.35
6-1	1.57	1.46	1-21-22	120.48	119.65
1-21	1.35	1.33	1-2-29	63.870	62.280
21-22	0.96	0.84	1-6-28	121.23	120.83
2-29	0.82	0.75	2-3-29	60.250	60.000
3-23	1.36	1.22	2-3-23	112.50	111.34
23-24	0.95	0.90	3-23-24	124.55	123.05
6-28	1.05	1.00	4-3-23-24	0	0
4-5	1.60	1.55	5-6-28	121.29	120.84
5-19	1.45	1.38	3-4-7	124.16	123.75
4-7	1.54	1.49	4-7-20	117.91	116.39
7-8	1.62	1.53	4-5-19	115.13	114.42
8-9	1.52	1.46	4-7-8	120.20	118.69
9-19	1.50	1.37	7-8-9	116.06	114.83
9-31	0.91	0.83	8-9-19	120.56	118.91
7-20	1.23	1.11	9-19-5	127.54	122.75
8-25	1.48	1.32	7-8-20	121.88	118.35
25-26	0.98	0.93	7-8-25	94.950	92.380
8-30	1.06	1.00	8-25-26	127.81	125.69
9-10	1.51	1.49	8-30-25	62.110	60.125
10-11	1.47	1.35	8-9-31	73.330	71.962
11-12	1.34	1.28	9-19-31	47.220	45.371
12-13	1.46	1.39	9-10-11	121.51	119.84
13-14	1.34	1.27	10-11-12	121.59	120.05
14-15	1.46	1.35	11-12-13	119.62	118.46
15-10	1.34	1.28	12-13-14	119.24	117.83
12-16	1.35	1.30	13-14-15	120.60	119.03
16-18	0.96	0.91	14-15-10	120.84	119.56
13-17	1.35	1.33	11-12-16	118.48	117.02
17-27	0.96	0.93	12-16-18	120.98	120.00
14-33	1.05	1.02	12-13-17	120.66	119.34
15-32	1.04	1.00	13-17-27	120.86	112.45

Table 5.6 *Structural parameters of tannin structure.*

Bond length (Å)	PM3	AM1	Angle (Å)	PM3	AM1
1-2	1.47	1.40	1-2-3	149.49	148.8
1-3	1.46	1.38	1-3-4	63.53	63.03
3-4	1.61	1.49	3-4-5	146.58	145.86
4-5	1.62	1.55	4-5-6	89.08	88.90
5-6	1.62	1.52	5-6-2	144.42	144.33
6-2	1.61	1.48	6-2-1	65.86	64.48
2-11	1.41	1.33	1-2-11	82.20	80.05
11-12	0.96	1.00	2-11-12	108.47	107.62
3-7	1.52	1.47	3-7-10	79.44	79.13
7-8	1.36	1.26	3-4-7	80.32	80.00
8-9	0.96	0.99	7-8-10	84.69	83.26
7-10	1.23	1.18	7-8-9	113.12	112.81
5-15	1.41	1.37	4-5-15	66.52	66.01
15-16	0.96	0.99	5-15-16	108.53	108.23
6-13	1.41	1.40	5-6-13	106.37	106.09
13-14	0.96	0.99	6-13-14	110.19	118.45
			2-6-13-14	0	0

5.3.3 FTIR Analyses

The FTIR results of *Mimosa tenuiflora* (tannins and flavonoids) is shown in Table 5.7 in where can be appreciated that these results are very similar between PM3 and AM1 methods. At 5697, 5647, 5485, 5102 and 4514 cm^{-1} corresponds to aromatic C-H signals (flavonoids). Between 4932–4912 cm^{-1} is assigned to OH stretching (flavonoid). The sign at 3480 and 3473 cm^{-1} is attributed to C=O and C=C (flavonoid) [8]. At 2790 and 2675 cm^{-1} corresponds to C=C bond (tannins), between 1332 and 1412 cm^{-1} is assigned to OH (tannins). From 375 to 366 cm^{-1} is attributed to OH out of plane (tannins). Finally the sign at 46, 38 and 33 cm^{-1} corresponds to different minerals present in the *Mimosa tenuiflora* [9-10].

**Table 5.7** *FTIR results of Mimosa tenuiflora (flavonoids and tannins) attributed to PM3 and AM1 method.*

ASSIGNMENT	PM3 (FREQUENCIES CM^{-1})	AM1 (FREQUENCIES CM^{-1})
CH stretching (flavonoid)	5697, 5102, 4514	5647, 5485
OH stretching (flavonoid)	4912	4932
C=C (flavonoid)	3706, 3484	3684
C=O, C=C (flavonoid)	3480	3473
C=C (tannin)	2790	2675
C-C (flavonoid)	1845, 1613	1841
C-O (flavonoid)	1317	1296
OH (flavonoid and tannin)	1093	1060
OH (tannin)	1412	1332
OH out of plane (tannin)	375	366
Minerals (Zn, Cu, Mn, Mg, Fe)	46, 33	38

5.3.4 Electrostatic Potential

Electrostatic potentials were obtained through the application of the PM3 and AM1 methods, Figure 5.7 shows that the potentials have values of 0.555-0.067 and 1.001-0.70 eV, respectively, Both methods show that the nucleophillic regions (green color) are located in links OH of the flavonoid structure and tannins is due to the numerous phenol groups in the tannin structure. The main reaction of tannins is thought to be between the oxygen of the C=O bond (COOH group) in the tannins and the OH group of the flavonoids [11].

5.3.5 Molecular Orbitals

The results of molecular orbital using PM3 and AM1 methods for *Mimosa tenuiflora* is shows in Tables 5.8 and 5.9. These results are very similar between both methods. HOMO orbitals in flavonoids and the LUMO orbitals in the tannins play an important role in chemical reactivity of *Mimosa tenuiflora*. The results showed that, in consideration of the atomic charges and the distribution of HOMO, A-ring of the flavonoid structure is the nucleophilic center [12]. This is due to that the tannins are amphipathic molecules having both hydrophobic aromatic rings and hydrophilic hydroxyl groups. These two properties allow tannins to simultaneously bind at several sites on the surface of other molecules [13].
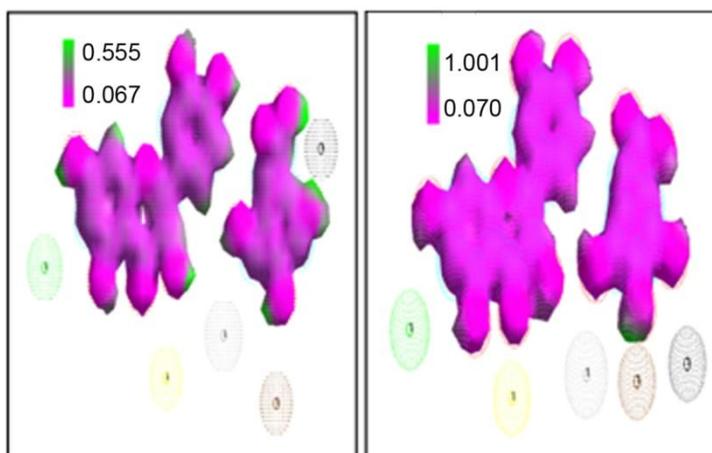
Figure 5.7 *Electrostatic potential of Mimosa tenuiflora (flavonoids and tannins) using (a) PM3 and (b) AM1 method.*

Table 5.8 *HOMO and LUMO orbitals for Mimosa tenuiflora (tannins and flavonoids) using PM3 method.*

ORBITAL	HOMO		LUMO	
	ENERGY (eV)	SYMMETRY (Å)	ENERGY (eV)	SYMMETRY (Å)
50	-16.72	0	3.814	0
20	-12-26	0	1.512	0
10	-11.41	0	0.192	0
5	-10.38	0	-0.750	0
-5	-0.747	0	-10.28	0
-10	0.199	0	-11.31	0
-20	1.516	0	-12.17	0
-50	3.814	0	-16.69	0

Table 5.9 *HOMO and LUMO orbitals for Mimosa tenuiflora (tannins and flavonoids) using AM1 method.*

ORBITAL	HOMO		LUMO	
	ENERGY (eV)	SYMMETRY (Å)	ENERGY (eV)	SYMMETRY (Å)
50	-16.79	0	3.53	0
20	-14.07	0	1.21	0
10	-11.56	0	-0.23	0
5	-10.37	0	-0.970	0
-5	-1.00	0	-10.29	0
-10	-0.22	0	-11.51	0
-20	1.22	0	-14.01	0
-50	3.55	0	-16.75	0

5.3.6 Conclusions

The high contents of flavonoids and tannins in the bark material are claimed to be responsible for potential wound-healing effects due to antimicrobial, anti-inflammatory and cicatrizing effects. It was determined by calculating the DG, molecular orbital and electrostatic potential that the reaction mechanism is through attractions by hydrogen bonds between the OH group of the flavonoids and the C=O group of tannins.

References

[1] USDA ARS. National Genetic Resources Program. Germplasm Resources Information Network - (GRIN) [Online Database]. National Germplasm Resources Laboratory, Beltsville, Maryland. URL: http://www.ars-grin.gov/cgi-bin/npgs/html/taxon.pl?24430.

[2] Lewis G P. Royal Botanic Gardens, Kew Legumes of Bahia, 369, 1987.

[3] Vepsäläïnen Jouko J, Seppo A, Mikko T, Nina R, Callaway J C. Isolation and characterization of yuremamine, a new phytoindole. *Planta Medica*, 71, 1053-1057, 2005.

[4] Rivera-Arce E, Gattuso M, Alvarado R, Zárate E, Agüero J, Feria I, Lozoya X. Pharmacognostical studies of the plant drug *Mimosae tenuiflorae cortex. Journal of Ethnopharmacology.* 113, 400–408, 2007.

[5] Octaviano de Souza R S, De Albuquerque U P, Monteiro J M, Cavalcanti de Amorim E L. Jurema-Preta (*Mimosa tenuiflora* [Willd.] Poir.): a review of its traditional use, phytochemistry and pharmacology. *Brazilian Archives of Biology and Technology*. 51(5), 937-947, 2008.

[6] Zippel J, Deters A, Hensel A. Arabinogalactans from *Mimosa tenuiflora* (Willd.) Poiret bark as active principles for wound-healing properties: Specific enhancement of dermal fibroblast activity and minor influence on HaCaT keratinocytes. *Journal of Ethnopharmacology*. 124, 391–396, 2009.

[7] Ramos G P, Frutos F, Giráldez J, Mantecón A R. Los Compuestos Secundarios De Las Plantas En La Nutrición De Los Herbívoros, *Arch. Zootec*. 47, 597-620. 1998.

[8] Martínez M A. Flavonoides. Tesis de Doctor, Universidad de Antioquia, Colombia. 1-76, 2005.

[9] Nnaji N J N, Okoye C O B, Obi-Egbedi N O, Ezeokonkwo M A, Ani J. Spectroscopic Characterization of Red Onion Skin Tannin and It's use as Alternative Aluminium Corrosion Inhibitor in Hydrochloric Acid Solutions. *International Journal of Electrochemical Science*. 8, 1735 – 1758, 2013.

[10] Hernández-Ortega Y, González-Mosquera D M. Extracción y Caracterización Preliminar de Taninos a Partir de Boldoa Purpurascens Cav. *Revista Cubana De Química*. XIX(2), 52-54, 2007.

[11] Mrak E M, Stewart G F, Chichester C O. Advances In Food Research, Ed. Elsevier, 13, 190, New-York, USA.

[12] Lu Z, Liao X, Zhang w, Tao Y, Shi B. Mechanism of Vegetable Tannin-aldehyde Combination Tannage. *The Journal of the American Leather Chemists Association*. 100(11), 432-437, 2005.

[13] Nelson S W. The Effects of Physical and Chemical Parameters on the Adsorption of Tannin to Grape Cell Wall Material, Thesis Master of Science in Viticulture and Enology. University of California (USA) 2011.

Chapter 6

Chitosan/PVP/Mimosa Tenuiflora

<div align="right">

Chapter 6

</div>

Chitosan/PVP/Mimosa Tenuiflora

<div align="center">

NORMA AUREA RANGEL-VÁZQUEZ[1]
FRANCISCO RODRÍGUEZ FÉLIX[2]

[1]División de Estudios de Posgrado e Investigación del Instituto Tecnológico de Aguascalientes, Ave. López Mateos # 1801 Ote. Fracc. Bona Gens CP. 20256 Aguascalientes, Aguascalientes, México
[2]Departamento de Investigación y Posgrado en Alimentos. Universidad de Sonora, Blvd. Luis Encinas y Rosales S/N Col. Centro, Hermosillo, Sonora, México

</div>

Abstract

Through the application of computational chemistry was determined a possible structure of the Chitosan/PVP/Mimosa tenuiflora using methods semi empirical (PM3 and AM1, respectively). It was observed the presence of hydrogen bonds to form a three-dimensional network. The results of both methods are very similar.

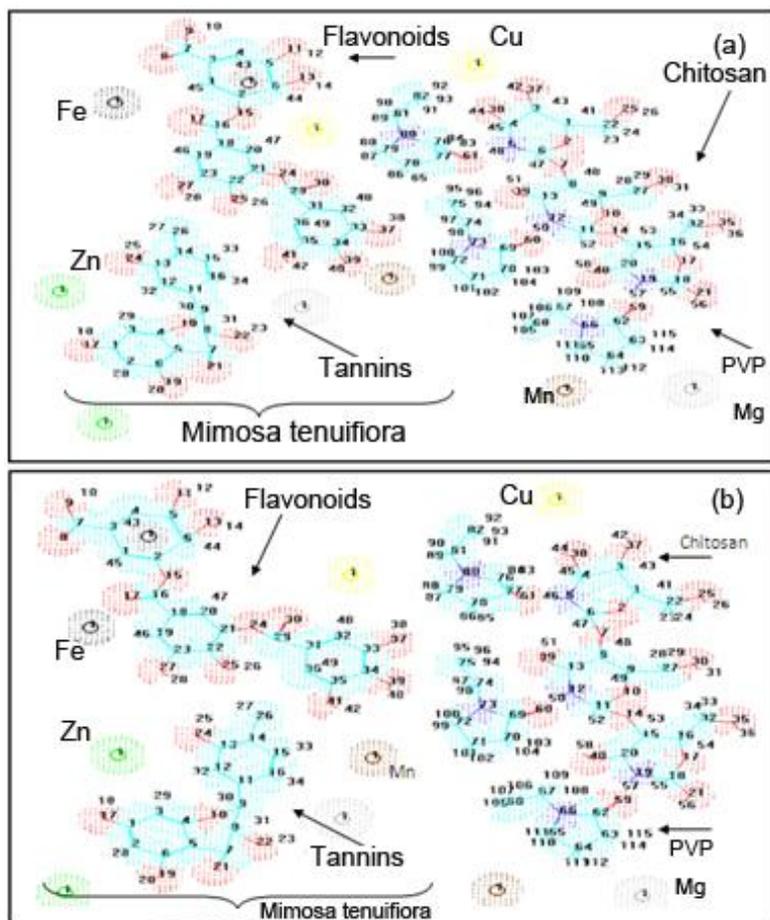*Keywords: Chitosan, PVP, Mimosa Tenuiflora, AM1, PM3, Simulation*

6.1 Simulation Results

6.1.1 Optimization Geometry

Figure 6.1 shows the geometry of optimization of Chitosan/PVP/Mimosa tenuiflora obtained through the application of the PM3 and AM1 semi-empirical methods, where the DG has negative values (Table 6.1) by causing the spontaneity of reaction. Furthermore, the formation of hydrogen bonds between the OH group (bond 37-38) of the *Mimosa tenuiflora* and hydrogen (bond 75-94) the PVP is observed, resulting in a three-dimensional network. It should be noted that DG values are similar between both methods.

Table 6.1 *Gibbs energy free for Chitosan/PVP/Mimosa tenuiflora structure.*

Method	ΔG (Kcal/mol)
AM1	- 6847
PM3	- 6992

Figure 6.1 *Geometry optimization (ΔG) of Chitosan/PVP/Mimosa tenuiflora, where (a) PM3 and (b) AM1 semi-empiric method.*

6.1.2 FTIR Analyses

As both high molecular weight blend components contain proton donor OH (Flavonoids) groups and proton acceptor (PVP, Tannins C=O), they may appear

to be miscible, due to the hydrogen bond formation [1]. Thus, the FTIR spectra of film blends, in the carbonyl stretching region of PVP at 1675-1670 cm^{-1}, and the hydroxyl stretching bands of chitosan near 3605–3584 cm^{-1} FTIR results obtained using PM3 and AM1 semi-empiric methods applied in Chitosan/PVP/*Mimosa tenuiflora* are presented in Table 6.2 The OH stretching (flavonoids) is assigned in the region of 6715-6300 cm^{-1}, between 6004-5987 corresponding to CH and OH stretching of chitosan [2]. The sign between 4469-4460 cm^{-1} clearly indicates strong intermolecular interactions between chitosan/PVP/*Mimosa tenuiflora*.

Table 6.2 *FTIR results of Chitosan/PVP/Mimosa tenuiflora (flavonoids and tannins) attributed to PM3 and AM1 semi-empiric method.*

ASSIGNMENT	PM3 (FREQUENCIES CM^{-1})	AM1 (FREQUENCIES CM^{-1})
OH stretching (Flavonoids)	6725-6581	6715 - 6398
CH and OH stretching (Chitosan)	6004	5987
CH (Chitosan) CH (CH$_2$-CH$_2$) (PVP)	5836	5784
CH asymmetric stretching (CH$_2$-OH) (Chitosan)	5412	5420
CH asymmetric stretching (PVP)	5203	5163
CH (Chitosan and PVP rings)	4827	4769
OH and CH (Chitosan, Flavonoids and Tannins)	4469	4460
C-H (Chitosan ring)	4101	4021
C=C (Flavonoids and tannins)	3716	3632
O-H (Chitosan)	3605	3584
C=C (Flavonoids)	3584	3522
C-C (PVP ring)	3309	3269
C=O (PVP)	3065	3058
C=O (Flavonoids)	2876	2858
CH=CH (Tannins)	2593	2551
C-C (PVP and Chitosan)	2441	2397
C-C (PVP ring)	2109	2038
C=O (PVP)	1675	1670
C-C, C-N, C-O (PVP and Chitosan)	1674	1604
C-O, C-C (Flavonoids)	1349	1316
CH (Tannins)	1007	1000
C-C and C-O out of plane (Chitosan)	451	444

6.1.3 Electrostatic Potential

Figure 6.2 shows the electrostatic potential of Chitosan/PVP/*Mimosa tenuiflora* obtained through the application of the PM3 and AM1 semi-empirical methods. Shows that the values vary from 4.212-0.082 and 4.891-0.084 respectively, these results prove the formation of hydrogen bonds between NH (chitosan) with C=O (PVP) and OH of flavonoids with the CH_2-CH_2 of the PVP obtained as well the formation of three-dimensional network. There is a region of the flavonoid structure presents a green color characteristic of a nucleophilic region, It should be noted that it is staining also occurs in the CH of the PVP bond.
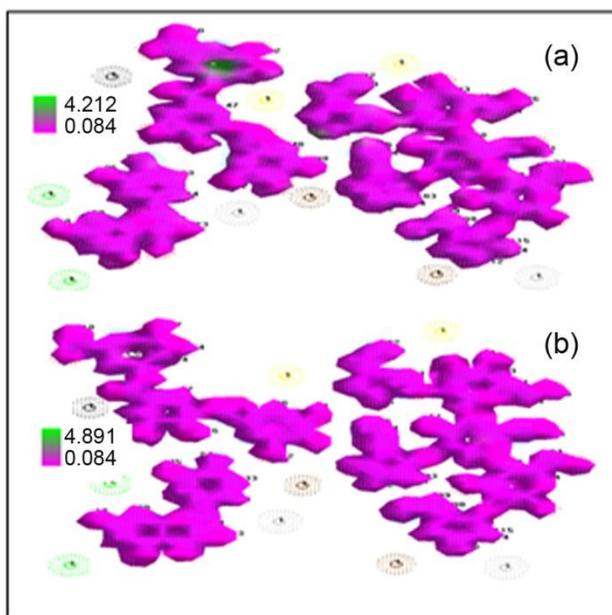
Figure 6.2 *Electrostatic potential of Chitosan/PVP/Mimosa tenuiflora (flavonoids and tannins) using (a) PM3 and (b) AM1 method.*

6.1.4 Molecular Orbitals

Tables 6.3 and 6.4 show values of the molecular orbitals (HOMO and LUMO) obtained through the application of the semi-empirical methods (PM3 and AM1, respectively). Shown that orbital HOMO compared their respective LUMO in each method is verified the spontaneity of reaction as well as the formation of hydrogen bonds for the three-dimensional network that is shown in Figure 6.3.

Table 6.3 *HOMO and LUMO orbitals for Chitosan/PVP/Mimosa tenuiflora (tannins and flavonoids) using PM3 semi-empiric method.*

ORBITAL	HOMO		LUMO	
	ENERGY (eV)	SYMMETRY (Å)	ENERGY (eV)	SYMMETRY (Å)
50	-13.26	23	-1.00	173
20	-12.99	26	-11.57	354
10	-12.94	154	-12.75	344
5	-12.93	158	-12.79	339
-5	-12.80	338	-12.93	159
-10	-12.76	343	-12.94	155
-20	-11.61	353	-12.98	25
-50	-1.00	173	-13.26	22

Table 6.4 *HOMO and LUMO orbitals for Chitosan/PVP/Mimosa tenuiflora (tannins and flavonoids) using AM1 semi-empiric method.*

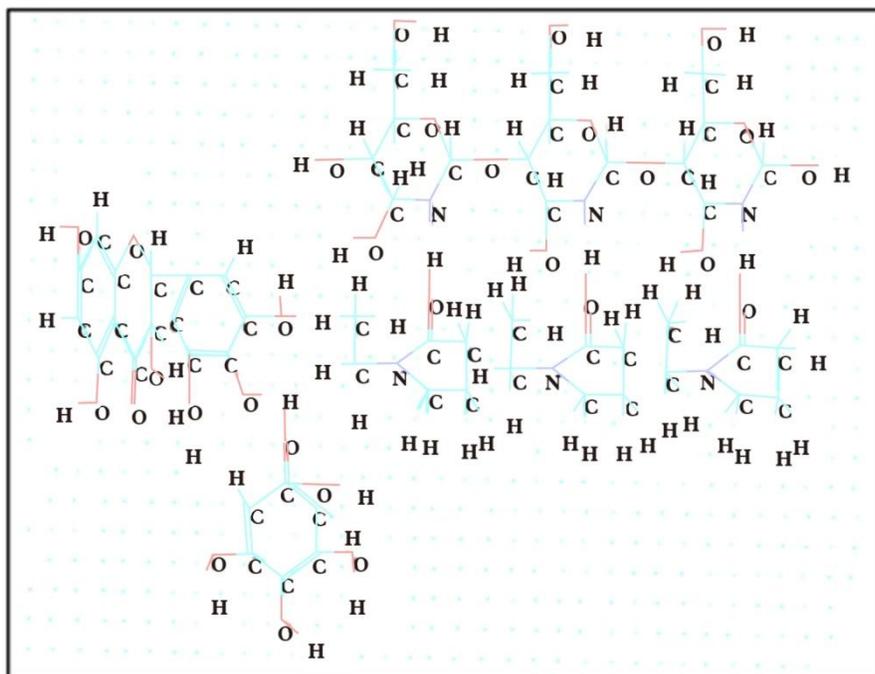| ORBITAL	HOMO		LUMO	
	ENERGY (eV)	SYMMETRY (Å)	ENERGY (eV)	SYMMETRY (Å)
50	-13.20	21	-1.01	174
20	-12.91	23	-11.60	351
10	-12.92	152	-12.73	342
5	-12.95	159	-12.82	339
-5	-12.83	340	-12.95	159
-10	-12.77	344	-12.92	152
-20	-11.60	351	-12.90	22
-50	-1.01	174	-13.20	21

Figure 6.3 *Three-dimensional network of Chitosan/PVP/Mimosa tenuiflora.*

6.1.5 Conclusions

Gibbs free energy determined the spontaneity of reaction through the application of both semi-empirical methods. Also the main signals of FTIR were obtained. With the molecular orbital and electrostatic potentials determined the formation of hydrogen bonds which were tested with the obtaining of the nucleophilic areas in the structure. These results are very similar in both methods.

References

[1] Lewandowska K. Miscibility and interactions in chitosan acetate/poly(N-vinylpyrrolidone) blends. *Thermochicica Acta.* 517(1-2), 90-97, 2011.

[2] Thakur A, Wanchoo R K. Preparation and Characterization of pH Sensitive Semi-Interpenetrating Polymer Networks of Chitosan and Polyvinylpyrrolidone. *International Conference on Agricultural, Environment and Biological Sciences*. 14-17. 2012.

List of Abbreviations

AIBN	Azobisisobutyronitrile
AM1	Austin model 1
AMBER	Assisted Model Building with Energy Refinement
CT	Charge transfer
ΔG	Gibbs free energy
%DD	Degree of deacetylation
eV	Electron-volt
FTIR	Fourier transform infrared spectroscopy
HOMO	Highest energy occupied molecular orbital
J	Joule
LUMO	Lowest energy occupied molecular orbital
MC	Mannosylated chitosan
MESP	Molecular electrostatic potential
MNDO	Modified Neglect of Diatomic Overlap
MT	*Mimosa tenuiflora*
NMR	Nuclear Magnetic Resonance
MO	Molecular orbital
PM3	Parametrization model 3
PPP	Pariser–Parr–Pople method
PVP	Polyvinylpyrrolidone

Computational Chemistry Applied in the Analyses of Chitosan/ Polyvinylpyrrolidone/ *Mimosa Tenuiflora*

Modeling is the process of producing a model; a model is a representation of the construction and working of some system of interest. A model is similar to but simpler than the system it represents. One purpose of a model is to enable the analyst to predict the effect of changes to the system. On the one hand, a model should be a close approximation to the real system and incorporate most of its salient features. On the other hand, it should not be so complex that it is impossible to understand and experiment with it. A good model is a judicious tradeoff between realism and simplicity.

To order additional copies of this book, please contact:
Science Publishing Group
service@sciencepublishinggroup.com
www.sciencepublishinggroup.com

Price: US $80